CHEMISTRY OF MATERIALS
Cite This: Chem. Mater. 2020, 32, 953−968
Article
pubs.acs.org/cm

Burying the Inverted Surface Dipole: Self-Assembled Monolayers Derived from Alkyl-Terminated Partially Fluorinated Alkanethiols

Maria D. Marquez, Oussama Zenasni, Daniela Rodriguez, Tianlang Yu, Siwakorn Sakunkaewkasem, Fabiana Toro Figueira, Arkadiusz Czader, Steven Baldelli, and T. Randall Lee*

Departments of Chemistry and Chemical Engineering and the Texas Center for Superconductivity, University of Houston, Houston, Texas 77204-5003, United States

Supporting Information

ABSTRACT: The direction and magnitude of surface dipoles directly affect the interfacial properties and can be tuned through molecular design. This article examines the effect of a hydrocarbon−fluorocarbon, "HC−FC", dipole on the structural and interfacial properties of self-assembled monolayers (SAMs) as the dipole is buried into the film. A series of selectively fluorinated alkanethiols with a progressively extended alkyl chain atop six fluorocarbons and an alkyl spacer of 11 hydrocarbons, $H(CH_2)_n(CF_2)_6(CH_2)_{11}SH$, where n = 1−7 (**HnF6H11SH**) were prepared and used to generate SAMs on evaporated gold, allowing for the systematic burying of the HC−FC dipole into the film. Structural analyses of the films revealed well-ordered films with slight disorder/loose packing in the top alkyl chains. In addition, odd−even effects were observed in the orientation and wettability of the SAMs corresponding to the number of carbon atoms in the top alkyl chain, leading to the conclusion that the fluorinated segment behaves as a surrogate surface. As for the effect of the dipole on the wetting behavior of the films, the effect appears to be minimized after three methylene units; however, the structural features of the monolayers were also found to influence the wettability of the films.

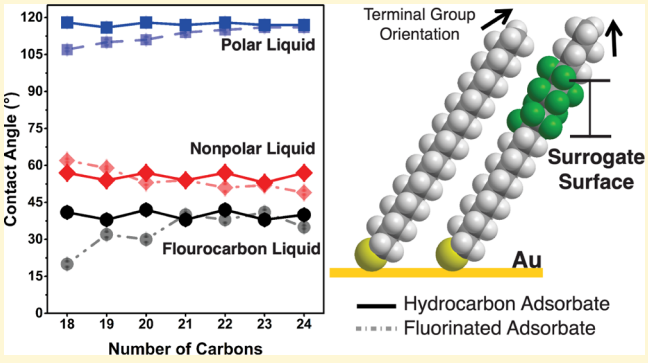

INTRODUCTION

Recent advances in nanotechnology have benefitted from the use of fluorinated organic thin films. Properties inherent to fluorocarbons allow them to be a leading candidate for nanoscale applications that include their use as lubricants for nanoelectromechanical systems and microelectromechanical systems.[1−3] The lubricant of choice for these types of systems has included partially fluorinated alkylsilanes in the form of fluorinated self-assembled monolayers (FSAMs). A better understanding of these robust films, with properties such as low adhesion and thermal stability, has been gained from studies regarding the structural/compositional features of these monolayers at the interface.[3−7] For example, multiple reports have described greater frictional properties for perfluorinated monolayer films on silica when compared to those of Teflon.[3,8] Moreover, perfluorinated coatings can alter the work function of electrodes, leading to a reduction in the charge-transfer barrier between the electrode and an overlying conjugated polymer.[9−12] Nevertheless, fluorinated thin films enjoy widespread use in applications beyond those of mechanical and electronic devices. In particular, fluorinated adsorbates have been used to generate antifouling coatings that inhibit the adsorption of biomaterials.[13,14]

Self-assembled monolayers (SAMs) generated by the adsorption of alkanethiols on gold continue to be widely used as model systems to investigate how the molecular features of an adsorbate influence the physical properties of the investigated films.[15−18] Several synthetic routes have evolved from research involving partially fluorinated alkanethiols in efforts to impart specifically desired properties into thin films.[4,19] Notably, the physical properties of SAMs derived from a series of fluorinated alkanethiols of the form $CF_3(CF_2)_n(CH_2)_2SH$ are dictated by the large perfluorinated segment rather than the short hydrocarbon spacer.[20−23] Insights into the role that limited levels of fluorination play in the interfacial properties of such films have been gained by the use of uniquely structured fluorinated adsorbates.[24−29] Lee and co-workers, for example, have shown the dependence of physical properties on the degree of fluorination by forming SAMs from partially fluorinated molecules of the form $CF_3(CF_2)_n(CH_2)_{11}SH$ where n = 1−10 (**FnH11SH**).[24−27] Moreover, the alkyl spacers of the SAMs largely dictate the structural features of the minimally fluorinated films, such as the relative crystallinity and packing density.[30,31] In addition, the improved thermal stability of fluorinated SAMs appears to depend on the enhanced van der Waals (vdW) interactions

Received: July 20, 2019
Revised: December 22, 2019
Published: December 23, 2019

Downloaded via UNIV OF HOUSTON MAIN on July 2, 2020 at 16:28:16 (UTC).
See https://pubs.acs.org/sharingguidelines for options on how to legitimately share published articles.

© 2019 American Chemical Society

DOI: 10.1021/acs.chemmater.9b02887
Chem. Mater. 2020, 32, 953−968

between the alkyl spacers that increases with increasing chain length, giving the films their high degree of conformational order.[27]

In a recent study,[32] we introduced methyl-terminated partially fluorinated SAMs of the form $CH_3(CF_2)_6(CH_2)_nSH$, where n = 10−13 (**H1F6HnSH**), as the first examples of fluorinated thin films with an inverted oriented surface dipole (i.e., HC−FC dipole, representing the hydrocarbon−fluorocarbon junction) at the terminal interface. These films, which represent a poignant example of manipulating the interfacial energies of monolayers using surface dipoles, exhibit lower contact angles by polar liquids than CF_3-terminated SAMs;[32,33] in addition, the methyl-terminated FSAMs display higher contact angles than their hydrocarbon analogs. However, the impact of these studies lies in the ability of the films to exhibit odd−even effects that are opposite to the those observed in CF_3-terminated films when in contact with polar protic liquids. In such liquids, the intermolecular H-bonds restrain the molecules from adopting a more favorable interfacial orientation (based on polarity) in the presence of the inverted surface dipole, as shown in Figure 1.

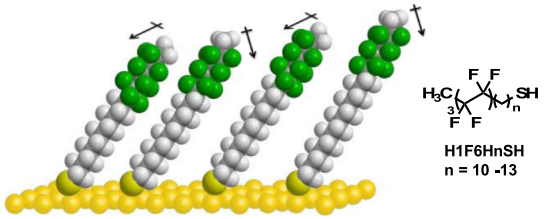

Figure 1. Illustration of oriented dipoles and their direction in SAMs generated from **H1F6HnSH** on gold.

In addition to the inverted odd−even effect observed for the **H1F6HnSH** FSAMs, the underlying perfluorinated segment in these adsorbates renders the films more oleophobic than their all-hydrocarbon counterparts. Additionally, the wetting behavior of various nonpolar liquids indicates that the orientation of the HC−FC dipole dictates the oleophobic character of the films through changes in the degree by which the underlying CF_2 units are exposed at the interface.

Building on our earlier work, the current study aims to draw a clearer conceptualization of the extent of the influence of the HC−FC inverted dipole. To this end, we designed, synthesized, and generated monolayer thin films from a series of alkyl-capped partially fluorinated alkanethiols of the structures $H(CH_2)_n(CF_2)_6(CH_2)_{11}SH$ (**HnF6H11SH**, where n = 1−7). Depictions of the partially fluorinated films examined in this study are shown in Figure 2 along with their fully hydrocarbon analogs. This study sought to determine the length of the top hydrocarbon segment beyond which the HC−FC dipole ceases to influence the interfacial energetics of the system.

We also wished to evaluate the effect of the extended alkyl moiety on the structural features of the fluorinated thin films. Along with the new adsorbates, we also describe studies of a series of normal alkanethiol SAMs $H(CH_2)_mSH$ (**HmSH**, where m = 18−24) to serve as reference films in our efforts to evaluate the structural and interfacial properties of the FSAMs generated from **HnF6H11SH**. SAMs formed from **HnF6H11SH** and the reference **HmSH** adsorbates were analyzed using ellipsometry, X-ray photoelectron spectroscopy (XPS), polarization modulation infrared reflection−adsorption

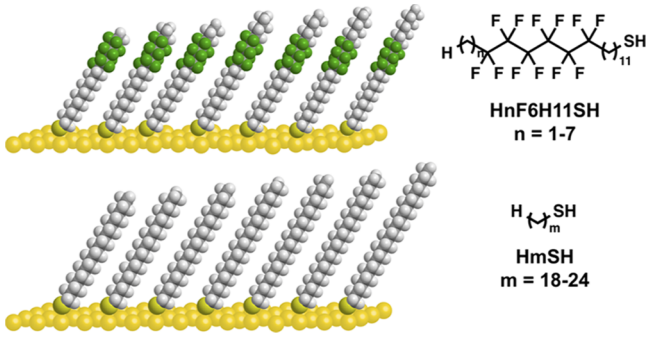

Figure 2. Schematic representation of SAMs generated from the **HnF6H11SH** (top) and **HmSH** (bottom) series.

spectroscopy (PM-IRRAS), vibrational sum frequency generation (SFG) spectroscopy, and contact angle goniometry.

EXPERIMENTAL SECTION

Materials. We purchased gold shot (99.999%; Americana Precious Metals), chromium rods (99.9%; R. D. Mathis Company), polished single-crystal silicon(100) wafers (Silicon Wafer Enterprises) from the indicated suppliers. Diethyl ether (Et_2O) and tetrahydrofuran (THF) were purchased from Avantor Performance Materials (Macron Chemicals and J. T. Baker), and were dried by distilling over calcium hydride (Sigma-Aldrich). Methanol (MeOH), acetone, and hexanes (from Avantor Performance Materials); ethyl acetate and dichloroethane (DCE) (from Sigma-Aldrich) were either used as received or degassed by purging with argon gas.

Azobisisobutyronitrile (AIBN), methanesulfonyl chloride (MsCl), lithium aluminum hydride ($LiAlH_4$), allyl alcohol, triethylamine (Et_3N), palladium on carbon (Pd/C), potassium thioacetate (KSAc), tetrabutylammonium fluoride solution, and methyl 10-undecenoate were all purchased from Sigma-Aldrich and used as received. 1,6-Diiodoperfluorohexane (Synquest Labs), 4-bromo-1-butene and 5-bromo-1-pentene (TCI America), 7-bromohept-1-ene (Oakwood), and 6-bromohex-1-ene (Matrix Scientific) were used as received. Sulfuric acid (H_2SO_4; J. T. Baker) and hydrochloric acid (HCl); potassium iodide (KI—EMD Chemicals); zinc dust (Fischer); glacial acetic acid (AcOH; Mallinckrodt Chemicals) were all used as received.

The adsorbate 1-octadecanethiol (**H18SH**) was purchased from Sigma-Aldrich and used as received. The adsorbates 1-nonadecanethiol (**H19SH**), 1-eicosanethiol (**H20SH**), 1-henicosanethiol (**H21SH**), 1-docosanethiol (**H22SH**), 1-tricosanethiol (**H23SH**), 1-tetracosanethiol (**H24SH**), and 12,12,13,13,14,14,15,15,16,16,17,17-dodecafluorooctadecane-1-thiol (**H1F6H11SH**) were synthesized according to literature procedures.[31,32,34,35]

Synthesis of Terminally Alkylated Partially Fluorinated Alkanethiols. As detailed below, the adsorbate 12,12,13,13,14,14,15,15,16,16,17,17-dodecafluorononadecane-1-thiol (**H2F6H11SH**) was synthesized according to Scheme 1; the adsorbate 12,12,13,13,14,14,15,15,16,16,17,17-dodecafluoroeicosane-1-thiol (**H3F6H11SH**) was synthesized according to Scheme 2; and the adsorbates 12,12,13,13,14,14,15,15,16,16,17,17-dodecafluorohenicosane-1-thiol (**H4F6H11SH**), 12,12,13,13,14,14,15,15,16,16,17,17-dodecafluorodocosane-1-thiol (**H5F6H11SH**), 12,12,13,13,14,14,15,15,16,16,17,17-dodecafluorotricosane-1-thiol (**H6F6H11SH**), and 12,12,13,13,14,14,15,15,16,16,17,17-dodecafluorotetracosane-1-thiol (**H7F6H11SH**) were synthesized according to Scheme 3.

Methyl 12,12,13,13,14,14,15,15,16,16,17,17-Dodecafluoro-10,17-diiodoheptadecanoate (1). In a 100 mL Schlenk flask, the starting materials 1,6-diiodoperfluorohexane (6.00 g; 10.8 mmol), AIBN (10 mol %), and methyl 10-undecenoate (1.83 g; 9.21 mmol) were dissolved in 20 mL of DCE. The system was degassed with three cycles of a standard freeze−pump−thaw procedure, and the mixture was heated to 85 °C for 5 h. After cooling to rt, the solvent was

DOI: 10.1021/acs.chemmater.9b02887
Chem. Mater. 2020, 32, 953−968

Scheme 1. Synthesis of 12,12,13,13,14,14,15,15,16,16,17,17-Dodecafluorononadecane-1-thiol (H2F6H11SH)

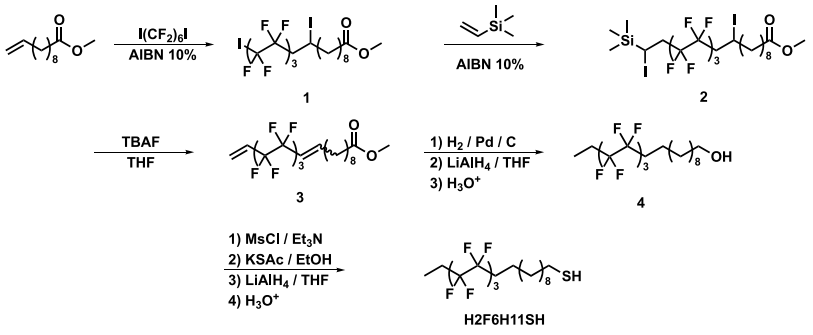

Scheme 2. Synthesis of 12,12,13,13,14,14,15,15,16,16,17,17-Dodecafluoroeicosane-1-thiol (H3F6H11SH)

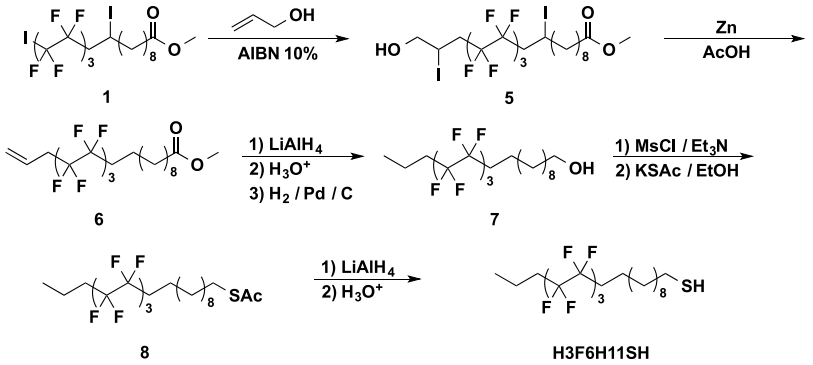

Scheme 3. Synthesis of 12,12,13,13,14,14,15,15,16,16,17,17-Dodecafluorohenicosane-1-thiol (H4F6H11SH), 12,12,13,13,14,14,15,15,16,16,17,17-Dodecafluorodocosane-1-thiol (H5F6H11SH), 12,12,13,13,14,14,15,15,16,16,17,17-Dodecafluorotricosane-1-thiol (H6F6H11SH), and 12,12,13,13,14,14,15,15,16,16,17,17-Dodecafluorotetracosane-1-thiol (H7F6H11SH)

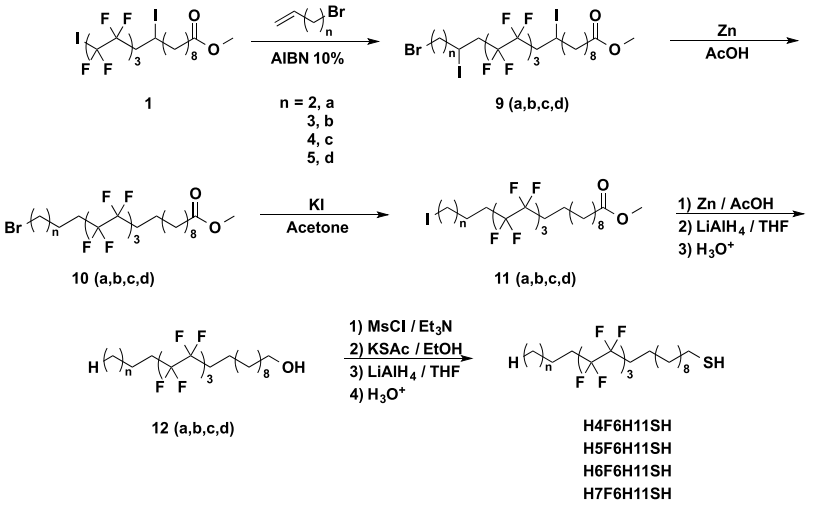

removed by rotary evaporation, and the product was purified by silica gel chromatography using hexanes/ethyl acetate (95:5) as the eluent to give methyl 12,12,13,13,14,14,15,15,16,16,17,17-dodecafluoro-10,17-diiodoheptadecanoate (**1**) in 56% yield. ^{1}H NMR (600 MHz, $CDCl_3$): δ 4.32 (m, 1H), 3.66 (s, 3H), 2.70−2.95 (m, 2H$_2$), 2.30 (t, J = 7.56 Hz, 2H), 1.71−1.85 (m, 2H), 1.51−1.63 (m, 4H), 1.24−1.42 (m, 8H). ^{19}F NMR (565 MHz, $CDCl_3$): δ −58.8 (m, 2F), −111.8 to −115.2 (m, 4F), −120.91 (m, 2F), −121.45 (m, 2F), −123.50 (m, 2F).

*Methyl 12,12,13,13,14,14,15,15,16,16,17,17-Dodecafluoro-10,19-diiodo-19-(trimethylsilyl)nonadecanoate (**2**).* In a 100 mL Schlenk flask, *F*-iodoester **1** (2.75 g; 3.6 mmol), trimethyl(vinyl)silane (0.80 mL; 5.4 mmol), and AIBN (10%) were dissolved in 20 mL of DCE. The mixture was degassed with three standard freeze−pump−thaw cycles and then warmed to 85 °C until consumption of the starting alkene. Afterward, rotary evaporation was used to remove the solvent, and the product was purified by chromatography on silica gel using hexanes/ethyl acetate (95:5) as the eluent to give the intermediate silane in 99% yield. ^{1}H NMR (400 MHz, $CDCl_3$): δ 4.29−4.36 (m, 1H), 3.66 (s, 3H), 3.19−3.22 (m, 1H), 2.50−2.99 (m, 4H), 2.30 (t, J = 7.66 Hz, 2H), 1.71−1.86 (m, 2H), 1.58−1.63 (m, 2H), 1.21−1.43 (m, 10H), 0.19 (s, 9H). ^{19}F NMR (376 MHz, $CDCl_3$): δ −115.7 to −111.2 (m, 4F, broad), −121.6 (m, 4F), −123.61 (m, 4F).

*Methyl 12,12,13,13,14,14,15,15,16,16,17,17-Dodecafluorononadeca-10,18-dienoate (**3**).* In a 100 mL round bottom flask,

DOI: 10.1021/acs.chemmater.9b02887
Chem. Mater. 2020, 32, 953−968

compound **2** (3.03 g; 3.55 mmol) was dissolved in 50 mL of distilled THF and cooled to 0 °C. Once cooled, 1 M TBAF solution (14.2 mL; 14.2 mmol) was added dropwise to the flask. The mixture was allowed to stir at rt for 16 h. Afterward, the reaction was quenched with 50 mL of 1 M HCl. The product was extracted with Et_2O (3 × 100 mL), and the organic layer washed with both water (2 × 100 mL) and brine (1 × 100 mL), and then dried with $MgSO_4$. After the solid was filtered off, the solution was passed through a short plug of silica gel, and then rotary evaporation was used to remove the solvent to give **3**, which was carried on to the next step without further purification. ^{1}H NMR (600 MHz, $CDCl_3$): δ 6.36−6.40 (m, 1H), 5.93−6.03 (m, 2H), 5.77−5.84 (m, 1H), 5.59 (q, J = 13.06 Hz, 1H), 3.66 (s, 3H), 2.30 (t, J = 7.21 Hz, 2H), 2.18 (m, 2H), 1.60−1.62 (m, 2H), 1.42−1.47 (m, 2H), 1.19−1.29 (m, 7H). ^{19}F NMR (565 MHz, $CDCl_3$): δ −111.1 (m, 2F), −113.7 (m, 2F), −121.5 (m, 4F), −123.6 (m, 4F).

*12,12,13,13,14,14,15,15,16,16,17,17-Dodecafluorononadecan-1-ol (**4**).* A slurry of Pd/C (10 mol %) in anhydrous MeOH (15 mL) was prepared in an oven-dried two-neck round bottom flask. The slurry was evacuated, refilled with H_2, and stirred for 20 min. Afterward, a solution of dissolved diene **3** (1.93 g; 3.69 mmol) in MeOH (20 mL) was transferred into the slurry. The mixture was stirred at rt for 48 h, refilling the flask with H_2 as necessary. Afterward, the mixture was diluted with Et_2O (200 mL) and filtered through a Celite pad. The solvent was then removed to give the ethyl-terminated partially fluorinated ester, which was used in the next step without purification. The crude ester (1.95 g; 3.69 mmol) was dissolved in dry THF (50 mL) and added dropwise to a stirred slurry of $LiAlH_4$ (0.218 g; 5.75 mmol) at 0 °C. The mixture was then allowed to warm to rt and stirred for 6 h. The reaction was quenched at 0 °C with H_2O (10 mL) and acidified with 2 M HCl (20 mL). The compound was extracted with Et_2O (3 × 100 mL), and the organic layer washed with both water (1 × 100 mL) and brine (1 × 100 mL), dried with $MgSO_4$, and the solvent removed by rotary evaporation. The crude alcohol was purified using silica gel chromatography with hexanes/ethyl acetate (80:20) as the eluent to give alcohol **4** in 82% yield from the iodosilane. ^{1}H NMR (600 MHz, $CDCl_3$): δ 3.64 (q, J = 6.19 Hz, 2H), 1.99−2.17 (m, 4H), 1.54−1.61 (m, 4H), 1.25−1.36 (m, 14H), 1.19 (t, J = 5.5 Hz, 1H), 1.14 (t, J = 7.56 Hz, 3H). ^{19}F NMR (565 MHz, $CDCl_3$): δ −114.4 to −114.3 (m, 2F), −116.3 to −116.2 (m, 2F), −121.8 (m, 4F), −123.6 (m, 4F).

*12,12,13,13,14,14,15,15,16,16,17,17-Dodecafluorononadecane-1-thiol (**H2F6H11SH**).* Alcohol **4** (1.47 g; 2.95 mmol) was dissolved in anhydrous THF (75 mL), and at 0 °C Et_3N (1.3 mL; 9.3 mmol) was added. After stirring for 30 min, an aliquot of MsCl (0.7 mL; 1.5 mmol) was added to the flask, and the mixture was allowed to stir at rt for 6 h. Afterward, the reaction was quenched with cold H_2O (50 mL), and the product was extracted with Et_2O (3 × 100 mL). The organic layer was then washed with 1 M HCl (1 × 100 mL), water (1 × 100 mL), brine (1 × 100 mL), and dried with $MgSO_4$. The solvent was then removed by rotary evaporation, and the crude mesylate carried to the next step without purification. The crude mesylated alcohol (1.98 g; 3.42 mmol) and KSAc (1.180 g; 10.3 mmol) were dissolved in anhydrous EtOH (75 mL, previously degassed) and refluxed for 4 h. After cooling to rt, the reaction was quenched with H_2O (50 mL) and the product extracted with Et_2O (3 × 100 mL). The organic layers were combined and washed with H_2O (1 × 100 mL) and brine (1 × 100 mL), and dried with $MgSO_4$. After removal of the solvent by rotary evaporation, the crude thioacetate was carried to the next step without further purification. The crude thioacetate (1.6 g; 2.9 mmol) was dissolved in anhydrous THF (50 mL, previously degassed). Once dissolved, the solution was added to a slurry of $LiAlH_4$ (0.17 g; 4.5 mmol) in 10 mL of THF (previously degassed) at 0 °C. The mixture was stirred at rt for 6 h. Afterward, the reaction was quenched with H_2O (20 mL, previously degassed) at 0 °C and immediately acidified with 1 M H_2SO_4 (50 mL, previously degassed) until the pH of the solution was ∼1. The product was then extracted with Et_2O (3 × 100 mL), and the combined organic layers were washed with H_2O (1 × 100 mL) and brine (1 × 100 mL), and dried with $MgSO_4$. After removal of the solvent by rotary evaporation, the crude thiol was purified using silica gel chromatography with hexanes/ethyl acetate (99:1) as the eluent to give 12,12,13,13,14,14,15,15,16,16,17,17-dodecafluorononadecane-1-thiol (**H2F6H11SH**) in 88% yield. ^{1}H NMR (600 MHz, $CDCl_3$): δ 2.52 (q, J = 7.33 Hz, 2H), 2.15 (m, 4H), 1.56−1.63 (m, 4H), 1.27−1.43 (m, 14H), 1.33 (t, J = 7.90 Hz, 1H), 1.13 (t, J = 7.21 Hz, 3H). ^{19}F NMR (565 MHz, $CDCl_3$): δ −114.4 (m, 2F), −116.4 (m, 2F), −121.8 (m, 4F), −123.6 (m, 4F). ^{13}C NMR (125 MHz, $CDCl_3$): δ 34.1 (s), 31.0 (t, J = 22.18 Hz), 29.2−29.6 (m), 28.5 (s), 24.7 (t, J = 11.09 Hz), 24.5 (s), 20.2 (m), 4.6 (t, J = 4.44 Hz). Broad peaks at δ 109.4−120.6 are characteristic of a long perfluorocarbon chain.[26] HR-CI-MS, m/z: 515.1644 $[M - H]^+$.

*Methyl 12,12,13,13,14,14,15,15,16,16,17,17-Dodecafluoro-20-hydroxy-10,19-diiodoeicosanoate (**5**).* In a 100 mL Schlenk flask, *F*-iodoester **1** (0.85 g; 1.1 mmol), AIBN (10 mol %), and allyl alcohol (0.13 g; 2.2 mmol) were dissolved in 20 mL of DCE. The mixture was degassed with three standard freeze−pump−thaw cycles, and the reaction heated to 85 °C for 12 h. The solvent was then removed by rotary evaporation, and the product was purified by silica gel chromatography using hexanes/ethyl acetate (70:30) as the eluent system to give methyl 12,12,13,13,14,14,15,15,16,16,17,17-dodecafluoro-20-hydroxy-10,19-diiodoeicosanoate (**5**) in 93% yield. ^{1}H NMR (500 MHz, $CDCl_3$): δ 4.43 (m, 1H), 4.32 (m, 1H), 3.79 (m, 2H), 3.66 (s, 3H), 2.70−3.06 (m, 4H), 2.30 (t, J = 7.56 Hz, 2H), 2.06 (t, J = 6.87 Hz, 1H), 1.71−1.85 (m, 2H), 1.51−1.63 (m, 2H), 1.24−1.42 (m, 10H). ^{19}F NMR (470 MHz, $CDCl_3$): δ −111.2 to −114.9 (m, 4F), −121.6 (m, 4F), −123.6 (m, 4F).

*Methyl 12,12,13,13,14,14,15,15,16,16,17,17-Dodecafluoroeicos-19-enoate (**6**).* Compound **5** (0.85 g; 1.0 mmol) was dissolved in a solution of THF (20 mL) and glacial acetic acid (50 mL). Zinc dust (2.06 g; 31.4 mmol) was then added under a flow of argon, and the mixture was stirred at rt for 48 h. The mixture was then diluted with 200 mL of Et_2O and filtered through Celite. The filtrate was then washed with water (3 × 100 mL), saturated aqueous $NaHCO_3$ (1 × 100 mL), and brine (1 × 50 mL), and dried over $MgSO_4$. The solvent was removed by rotary evaporation to give methyl 12,12,13,13,14,14,15,15,16,16,17,17-dodecafluoroeicos-19-enoate (**6**) in 90% yield. ^{1}H NMR (500 MHz, $CDCl_3$): δ 5.79 (m, 1H), 5.32 (m, 2H), 3.66 (s, 3H), 2.84 (m, 2H), 2.29 (t, J = 7.56 Hz, 2H), 1.98−2.10 (m, 2H), 1.55−1.63 (m, 2H), 1.21−1.37 (m, 14H). ^{19}F NMR (470 MHz, $CDCl_3$): δ −113.2 (m, 2F), −114.3 (m, 2F), −121.8 (m, 4F), −123.2 (m, 2F), −123.6 (m, 2F).

*12,12,13,13,14,14,15,15,16,16,17,17-Dodecafluoroeicosan-1-ol (**7**).* Olefin **6** (0.51 g; 0.94 mmol) was dissolved in anhydrous THF (50 mL) and added dropwise to a stirring slurry of $LiAlH_4$ (0.107 g; 2.82 mmol) in THF (10 mL) at 0 °C. The mixture was then warmed to rt and stirred for 6 h under argon. Afterward, at 0 °C, the reaction was quenched with 20 mL of water, followed by the addition of 1 M aqueous HCl solution (20 mL). The mixture was then extracted with Et_2O (3 × 100 mL). The combined organic layers were washed with water (1 × 100 mL) and brine (1 × 100 mL), dried over $MgSO_4$, and evaporated to dryness by rotary evaporation. Crude alcohol was used in the next step without further purification.

The crude compound was dissolved in 30 mL of MeOH and added to a slurry of Pd/C (10%). The mixture was placed under 1 atm of hydrogen and stirred at rt for 12 h. The mixture was filtered through a pad of Celite and then washed with Et_2O (100 mL). After removal of the solvent, the product was purified by chromatography on silica gel using hexanes/ethyl acetate (70:30) as the eluent system to give 12,12,13,13,14,14,15,15,16,16,17,17-dodecafluoroeicosan-1-ol (**7**) in 66% yield. ^{1}H NMR (500 MHz, $CDCl_3$): δ 3.64 (t, J = 6.70 Hz, 2H), 1.98−2.08 (m, 4H), 1.55−1.65 (m, 6H), 1.14−1.41 (m, 14H), 1.01 (t, J = 7.22 Hz, 3H). ^{19}F NMR (470 MHz, $CDCl_3$): δ −114.4 (m, 4F), −121.8 (m, 4F), −123.7 (m, 4F).

*S-(12,12,13,13,14,14,15,15,16,16,17,17-Dodecafluoroeicosyl)-ethanethioate (**8**).* Alcohol **7** (0.32 g; 0.62 mmol) was dissolved in anhydrous THF (20 mL), and at 0 °C Et_3N (0.26 mL; 1.9 mmol) was added to the flask. After stirring for 30 min, MsCl (0.24 mL; 3.1 mmol) was added dropwise, and the mixture was allowed to stir at rt for 12 h. The reaction was then quenched with 50 mL of cold water, and the product was extracted with Et_2O (3 × 100 mL). The

DOI: 10.1021/acs.chemmater.9b02887
Chem. Mater. 2020, 32, 953−968

combined organic phases were washed with 1 M aqueous HCl (1 × 100 mL), water (1 × 100 mL), brine (1 × 100 mL), and dried with $MgSO_4$. The solvent was then removed by rotary evaporation, and the crude mesylate was used in the next step without purification.

The crude product and KSAc (0.345 g; 3.02 mmol) were dissolved in anhydrous ethanol (50 mL, previously degassed) and refluxed for 6 h. After cooling to rt, the reaction was quenched with H_2O (50 mL) and the product extracted with Et_2O (3 × 100 mL). The organic layers were combined and washed with H_2O (1 × 100 mL) and brine (1 × 100 mL), and dried with $MgSO_4$. After removal of the solvent by rotary evaporation, the crude thioacetate was purified by chromatography on silica gel (hexanes/ethyl acetate; 95:5) to give *S*-(12,12,13,13,14,14,15,15,16,16,17,17-dodecafluoroeicosyl)-ethanethioate (**8**) in 98% yield. ^{1}H NMR (500 MHz, $CDCl_3$): δ 2.85 (t, J = 7.39 Hz, 2H), 2.32 (s, 3H), 1.98−2.08 (m, 6H), 1.52−1.66 (m, 4H), 1.26−1.36 (m, 14H), 1.02 (t, J = 7.39 Hz, 3H). ^{19}F NMR (470 MHz, $CDCl_3$): δ −114.3 (m, 4F), −121.8 (m, 4F), −123.7 (m, 4F).

*12,12,13,13,14,14,15,15,16,16,17,17-Dodecafluoroeicosane-1-thiol (**H3F6H11SH**).* Thioacetate **8** (0.30 g; 0.52 mmol) was dissolved in anhydrous THF (30 mL). Once dissolved, the solution was added to a slurry of $LiAlH_4$ (0.059 g; 1.6 mmol) in THF (5 mL) at −10 °C. The mixture was stirred at ∼−10 °C for 6 h under argon. Afterward, the reaction was quenched with H_2O (20 mL, previously degassed) at 0 °C and immediately acidified with 1 M H_2SO_4 (50 mL, previously degassed) until the pH of the solution was ∼1. The product was then extracted with Et_2O (3 × 100 mL) and the combined organic layers washed with H_2O (1 × 100 mL) and brine (1 × 100 mL), and dried with $MgSO_4$. After removal of the solvent by rotary evaporation, the resulting thiol was purified by chromatography on silica gel (hexanes/ethyl acetate; 99:1) to give 12,12,13,13,14,14,15,15,16,16,17,17-dodecafluoroeicosane-1-thiol (**H3F6H11SH**) in 50% yield. ^{1}H NMR (600 MHz, $CDCl_3$): δ 2.51 (q, J = 7.45 Hz, 2H), 1.96−2.09 (m, 4H), 1.55−1.68 (m, 6H), 1.25−1.36 (m, 15H), 1.02 (t, J = 7.45 Hz, 3H). ^{19}F NMR (565 MHz, $CDCl_3$): δ −114.3 (m, 4F), −121.8 (m, 4F), −123.7 (m, 4F). ^{13}C NMR (150 MHz, $CDCl_3$): δ 34.2 (s), 33.0 (t, J = 22.18 Hz), 31.1 (t, J = 22.18 Hz), 29.2−29.6 (m), 28.5 (s), 24.8 (s), 20.3 (s), 13.9 (m), 13.8 (s). Broad peaks at δ 109.4−120.5 are characteristic of a long perfluorocarbon chain.[26] HR-CI-MS, m/z: 529.1797 $[M - H]^+$.

*Methyl 21-Bromo-12,12,13,13,14,14,15,15,16,16,17,17-dodecafluoro-10,19-diiodohenicosano-ate (**9a**).* In a 100 mL Schlenk flask, *F*-iodoester **1** (1.64 g; 2.18 mmol), AIBN (10 mol %), and 4-bromo-heptene (0.60 g; 4.4 mmol) were dissolved in 20 mL of DCE and degassed using three cycles of a standard freeze−pump−thaw procedure. After degassing, the reaction was run at 85 °C for 12 h. Afterward, the solvent was removed by rotary evaporation, and the crude product purified by silica gel chromatography using hexanes/ethyl acetate (90:10) as the eluent to give **9a** in 88% yield. ^{1}H NMR (500 MHz, $CDCl_3$): δ 4.49−4.51 (m, 1H), 4.30−4.35 (m, 1H), 3.66 (s, 3H), 3.59−3.61 (m, 1H), 3.46−3.51 (m, 1H), 2.75−3.04 (m, 4H), 2.30 (t, J = 7.56 Hz, 2H), 2.22−2.34 (m, 2H), 1.72−1.83 (m, 2H), 1.51−1.63 (m, 4H), 1.18−1.42 (m, 8H). ^{19}F NMR (476 MHz, $CDCl_3$): δ −110.5 to −114.8 (m, 4F), −121.5 (m, 4F), −123.5 (m, 4F). Compounds **9b**, **9c**, and **9d** were prepared using analogous methodology (vide infra).

*Methyl 22-Bromo-12,12,13,13,14,14,15,15,16,16,17,17-dodecafluoro-10,19-diiododocosanoate (**9b**).* Methyl 22-bromo-12,12,13,13,14,14,15,15,16,16,17,17-dodecafluoro-10,19-diiododocosanoate (**9b**) in 86% yield. ^{1}H NMR (500 MHz, $CDCl_3$): δ 4.30−4.34 (m, 2H), 3.66 (s, 3H), 3.43−3.45 (m, 2H), 2.73−2.92 (m, 4H), 2.30 (t, J = 7.56 Hz, 2H), 2.11−2.19 (m, 1H), 1.92−2.04 (m, 3H), 1.72−1.84 (m, 2H), 1.60−1.63 (m, 2H), 1.51−1.56 (m, 1H), 1.23−1.42 (m, 9H). ^{19}F NMR (476 MHz, $CDCl_3$): δ −111.2 to −114.8 (m, 4F), −121.6 (m, 4F), −123.6 (m, 4F).

*Methyl 23-Bromo-12,12,13,13,14,14,15,15,16,16,17,17-dodecafluoro-10,19-diiodotricosanoate (**9c**).* Methyl 23-bromo-12,12,13,13,14,14,15,15,16,16,17,17-dodecafluoro-10,19-diiodotricosanoate (**9c**) in 88% yield. ^{1}H NMR (500 MHz, $CDCl_3$): δ 4.30−4.35 (m, 2H), 3.66 (s, 3H), 3.42 (t, J = 6.7 Hz, 2H), 2.71−2.99 (m, 4H), 2.30 (t, J = 7.56 Hz, 2H), 1.68−1.98 (m, 6H), 1.51−1.63 (m, 4H), 1.24−1.42 (m, 10H). ^{19}F NMR (476 MHz, $CDCl_3$): δ −111.9 to −111.1 (m, 2F), −114.8 to −114.2 (m, 2F), −121.6 (m, 4F), −123.6 (m, 4F).

*Methyl 24-Bromo-12,12,13,13,14,14,15,15,16,16,17,17-dodecafluoro-10,19-diiodotetracosano-ate (**9d**).* Methyl 24-bromo-12,12,13,13,14,14,15,15,16,16,17,17-dodecafluoro-10,19-diiodotetracosano-ate (**9d**) in 90% yield. ^{1}H NMR (400 MHz, $CDCl_3$): δ 4.29−4.36 (m, 2H), 3.67 (s, 3H), 3.42 (t, J = 6.6 Hz, 2H), 2.69−2.99 (m, 4H), 2.31 (t, J = 7.56 Hz, 2H), 1.71−1.93 (m, 6H), 1.21−1.64 (m, 16H). ^{19}F NMR (376 MHz, $CDCl_3$): δ −111.2 (m, 1F), −111.9 to −111.8 (m, 2F), −114.2 (m, 2F), −114.9 (m, 1F), −121.6 (m, 4F), −123.6 (m, 4F).

*Methyl 21-Bromo-12,12,13,13,14,14,15,15,16,16,17,17-dodecafluorohenicosanoate (**10a**).* Intermediate **9a** (1.7 g; 1.9 mmol) was dissolved in a 500 mL round bottom flask in glacial acetic acid (100 mL); 20 mL of distilled THF was added in order to help the compound dissolve. Zn powder (3.77 g; 57.5 mmol) was added under the flow of argon with vigorous stirring. The mixture was allowed to stir at rt in the dark for 48 h. Afterward, the accumulated pressure was carefully released before opening the flask. The mixture was diluted with diethyl ether and filtered through a pad of Celite. The filtrate was then washed with a copious amount of water (10 × 100 mL), saturated $NaHCO_3$ solution (2 × 50 mL), brine (1 × 100 mL), and dried with $MgSO_4$. The solvent was then removed by rotary evaporation giving intermediate **10a** in 94% yield. ^{1}H NMR (500 MHz, $CDCl_3$): δ 3.66 (s, 3H), 3.43 (t, J = 6.70, 2H), 2.30 (t, J = 7.56, 2H), 2.13−1.91 (m, 6H), 1.78 (m, 2H), 1.62−1.54 (m, 4H), 1.35 (m, 12H). ^{19}F NMR (476 MHz, $CDCl_3$): δ −114.3 (m, 4F), −121.8 (m, 4F), −123.6 (m, 4F). Compounds **10b**, **10c**, and **10d** were prepared using analogous methodology (vide infra).

*Methyl 22-Bromo-12,12,13,13,14,14,15,15,16,16,17,17-dodecafluorodocosanoate (**10b**).* Methyl 22-bromo-12,12,13,13,14,14,15,15,16,16,17,17-dodecafluorodocosanoate (**10b**) in 96% yield. ^{1}H NMR (500 MHz, $CDCl_3$): δ 3.66 (s, 3H), 3.42 (t, J = 6.70 Hz, 2H), 2.30 (t, J = 7.56 Hz, 2H), 1.98−2.13 (m, 4H), 1.87−1.93 (m, 2H), 1.54−1.64 (m, 8H), 1.24−1.37 (m, 12H). ^{19}F NMR (476 MHz, $CDCl_3$): δ −114.3 (m, 4F), −121.8 (m, 4F), −123.6.

*Methyl 23-Bromo-12,12,13,13,14,14,15,15,16,16,17,17-dodecafluorotricosanoate (**10c**).* Methyl 23-bromo-12,12,13,13,14,14,15,15,16,16,17,17-dodecafluorotricosanoate (**10c**) in 92% yield. ^{1}H NMR (500 MHz, $CDCl_3$): δ 3.65 (s, 3H), 3.40 (t, J = 6.70 Hz, 2H), 2.29 (t, J = 7.56 Hz, 2H), 1.97−2.10 (m, 4H), 1.84−1.89 (m, 2H), 1.54−1.65 (m, 6H), 1.20−1.51 (m, 16H). ^{19}F NMR (476 MHz, $CDCl_3$): δ −114.3 (m, 4F), −121.6 (m, 4F), −123.1.

*Methyl 24-Bromo-12,12,13,13,14,14,15,15,16,16,17,17-dodecafluorotetracosanoate (**10d**).* Methyl 24-bromo-12,12,13,13,14,14,15,15,16,16,17,17-dodecafluorotetracosanoate (**10d**) in 93% yield. ^{1}H NMR (500 MHz, $CDCl_3$): δ 3.67 (s, 3H), 3.41 (t, J = 6.87 Hz, 2H), 2.30 (t, J = 7.73 Hz, 2H), 2.03−2.05 (m, 4H), 1.83−1.89 (m, 2H), 1.55−1.62 (m, 6H), 1.25−1.47 (m, 18H). ^{19}F NMR (476 MHz, $CDCl_3$): δ −114.3 (m, 4F), −121.8 (m, 4F), −123.6.

*Methyl 12,12,13,13,14,14,15,15,16,16,17,17-Dodecafluoro-21-iodohenicosanoate (**11a**).* The bromoester (1.33 g; 2.09 mmol) and potassium iodide (1.74 g; 10.5 mmol) were dissolved in 50 mL of acetone in a 100 mL round bottom flask. The mixture was then refluxed for 24 h. After cooling to rt, the solvent was removed by rotary evaporation, and the resulting residue was dissolved in Et_2O (200 mL). The organic layer was then washed with water (1 × 100 mL) and brine (1 × 100 mL), and dried with $MgSO_4$. Rotary evaporation was used to remove the solvent to give **11a** in 95% yield. ^{1}H NMR (500 MHz, $CDCl_3$): δ 3.66 (s, 3H), 3.20 (t, J = 6.87 Hz, 2H), 2.30 (t, J = 7.56 Hz, 2H), 1.98−2.10 (m, 4H), 1.91 (m, 2H), 1.71−1.78 (m, 2H), 1.54−1.63 (m, 4H), 1.20−1.43 (m, 12H). ^{19}F NMR (476 MHz, $CDCl_3$): δ −114.3 (m, 4F), −121.8 (m, 4F), −123.6 (m, 4F). Compounds **11b**, **11c**, and **11d** were prepared using an analogous methodology.

*Methyl 12,12,13,13,14,14,15,15,16,16,17,17-Dodecafluoro-22-iododocosanoate (**11b**).* Methyl 12,12,13,13,14,14,15,15,16,16,17,17-

DOI: 10.1021/acs.chemmater.9b02887
Chem. Mater. 2020, 32, 953−968

dodecafluoro-22-iododocosanoate (**11b**) in 97% yield. ^{1}H NMR (500 MHz, $CDCl_3$): δ 3.66 (s, 3H), 3.20 (t, J = 6.87 Hz, 2H), 2.30 (t, J = 7.56 Hz, 2H), 2.01−2.11 (m, 4H), 1.83−1.89 (m, 2H), 1.43−1.65 (m, 8H), 1.25−1.36 (m, 12H). ^{19}F NMR (476 MHz, $CDCl_3$): δ −114.3 (m, 4F), −121.8 (m, 4F), −123.6 (m, 4F).

*Methyl 12,12,13,13,14,14,15,15,16,16,17,17-Dodecafluoro-23-iodotricosanoate (**11c**).* Methyl 12,12,13,13,14,14,15,15,16,16,17,17-dodecafluoro-23-iodotricosanoate (**11c**) in 100% yield. ^{1}H NMR (500 MHz, $CDCl_3$): δ 3.66 (s, 3H), 3.18 (t, J = 7.04 Hz, 2H), 2.29 (t, J = 7.56 Hz, 2H), 1.97−2.10 (m, 4H), 1.80−1.86 (m, 2H), 1.54−1.64 (m, 6H), 1.27−1.47 (m, 16H). ^{19}F NMR (476 MHz, $CDCl_3$): δ −114.3 (m, 4F), −121.6 (m, 4F), −123.6 (m, 4F).

*Methyl 12,12,13,13,14,14,15,15,16,16,17,17-Dodecafluoro-24-iodotetracosanoate (**11d**).* Methyl 12,12,13,13,14,14,15,15,16,16,17,17-dodecafluoro-24-iodotetracosanoate (**11d**) in 99% yield. ^{1}H NMR (500 MHz, $CDCl_3$): δ 3.67 (s, 3H), 3.19 (t, J = 6.87 Hz, 2H), 2.30 (t, J = 7.73 Hz, 2H), 1.99−2.09 (m, 4H), 1.80−1.85 (m, 2H), 1.57−1.63 (m, 6H), 1.25−1.44 (m, 18H). ^{19}F NMR (470 MHz, $CDCl_3$): δ −114.3 (m, 4F), −121.8 (m, 4F), −123.6 (m, 4F).

*12,12,13,13,14,14,15,15,16,16,17,17-Dodecafluorohenicosan-1-ol (**12a**).* Intermediate **11a** (1.37 g; 2.00 mmol) was dissolved in a mixture of glacial acetic acid (100 mL) and THF (20 mL). The addition of zinc dust (1.98 g; 30.1 mmol) was performed under a flow of argon with vigorous stirring. The mixture was allowed to stir at rt for 48 h, at which point the mixture was diluted with Et_2O (200 mL) and filtered through a pad of Celite. The filtrate was then washed with H_2O (10 × 100 mL), saturated $NaHCO_3$ (2 × 50 mL), brine (1 × 100 mL), and dried with $MgSO_4$. Rotary evaporation was used to remove the solvent, and the crude product carried into the next step without further purification.

The resulting crude ester (0.916 g; 1.65 mmol) was dissolved in dry THF (50 mL) and added to a stirring slurry of $LiAlH_4$ (0.188 g; 4.94 mmol) at 0 °C. The mixture was allowed to stir at rt for 4 h under argon. The mixture was cooled to 0 °C, quenched with H_2O (20 mL), and acidified with 1 M HCl (50 mL). The solution was then extracted with Et_2O (3 × 100 mL). The combined Et_2O layers were washed with water (1 × 100 mL) and brine (1 × 100 mL), and dried with $MgSO_4$. Afterward, the solvent was removed by rotary evaporation, and the compound purified with silica gel chromatography using hexanes/ethyl acetate (80:20) as the eluent to give 12,12,13,13,14,14,15,15,16,16,17,17-dodecafluorotetracosan-1-ol (**12a**) in 76% yield. ^{1}H NMR (500 MHz, $CDCl_3$): δ 3.64 (t, J = 6.70 Hz, 2H), 1.98−2.10 (m, 4H), 1.55−1.58 (m, 6H), 1.28−1.41 (m, 16H), 0.95 (t, J = 7.22 Hz, 3H). ^{19}F NMR (476 MHz, $CDCl_3$): δ −114.3 (m, 4F), −121.8 (m, 4F), −123.6 (m, 4F). Compounds **12b**, **12c**, and **12d** were prepared using an analogous methodology.

*12,12,13,13,14,14,15,15,16,16,17,17-Dodecafluorodocosan-1-ol (**12b**).* 12,12,13,13,14,14,15,15,16,16,17,17-Dodecafluorodocosan-1-ol (**12b**) in 95% yield. ^{1}H NMR (500 MHz, $CDCl_3$): δ 3.63 (q, J = 6.30 Hz, 2H), 1.98−2.09 (m, 4H), 1.54−1.61 (m, 6H), 1.25−1.37 (m, 18H), 0.91 (t, J = 7.05 Hz, 3H). ^{19}F NMR (476 MHz, $CDCl_3$): δ −114.3 (m, 4F), −121.8 (m, 4F), −123.6 (m, 4F).

*12,12,13,13,14,14,15,15,16,16,17,17-Dodecafluorotricosan-1-ol (**12c**).* 12,12,13,13,14,14,15,15,16,16,17,17-Dodecafluorotricosan-1-ol (**12c**) in 40% yield. ^{1}H NMR (500 MHz, $CDCl_3$): δ 3.62−3.67 (m, 2H), 1.98−2.10 (m, 4H), 1.54−1.62 (m, 6H), 1.21−1.40 (m, 20H), 0.90 (t, J = 7.04 Hz, 3H). ^{19}F NMR (476 MHz, $CDCl_3$): δ −114.3 (m, 4F), −121.8 (m, 4F), −123.6 (m, 4F).

*12,12,13,13,14,14,15,15,16,16,17,17-Dodecafluorotetracosan-1-ol (**12d**).* 12,12,13,13,14,14,15,15,16,16,17,17-Dodecafluorotetracosan-1-ol (**12d**) in 76% yield. ^{1}H NMR (400 MHz, $CDCl_3$): δ 3.62−3.67 (q, J = 6.11 Hz, 2H), 1.97−2.11 (m, 4H), 1.53−1.63 (m, 6H), 1.28−1.36 (m, 22H), 1.19 (t, J = 5.27 Hz, 1H), 0.89 (t, J = 6.87 Hz, 3H). ^{19}F NMR (376 MHz, $CDCl_3$): δ −114.3 (m, 4F), −121.8 (m, 4F), −123.7 to −123.6 (m, 4F).

*12,12,13,13,14,14,15,15,16,16,17,17-Dodecafluorohenicosane-1-thiol (**H4F6H11SH**).* Alcohol **12a** (0.66 g; 1.2 mmol) was dissolved in 50 mL of anhydrous THF followed by cooling to 0 °C. Afterward, Et_3N (0.52 mL; 3.7 mmol) was added dropwise, and the solution was allowed to stir at 0 °C for 30 min. Subsequently, an aliquot of MsCl (0.48 mL; 6.2 mmol) was slowly added to the mixture. The mixture was warmed to rt and stirred for 6 h. The reaction was then quenched with ice-cold water (50 mL) followed by 1 M HCl (50 mL). The solution was then extracted with Et_2O (3 × 100 mL). The combined organic layers were then washed with 1 M HCl (1 × 100 mL), H_2O (1 × 100 mL), brine (1 × 100 mL), and dried with $MgSO_4$. Rotary evaporation was used to remove the solvent, and the resulting mesylated alcohol was used in the next step without further purification.

The crude mesylated alcohol (0.87 g; 1.4 mmol) and KSAc (0.819 g; 7.17 mmol) were dissolved in anhydrous ethanol (100 mL, previously degassed). The mixture was then refluxed for 4 h. Afterward, the solvent was removed by rotary evaporation, and the resulting residue was dissolved in Et_2O (200 mL). The organic layer was washed with water (1 × 100 mL) and brine (1 × 100 mL), dried with $MgSO_4$, and the solvent removed by rotary evaporation. The crude thioacetate was dried under high vacuum overnight and used in the next step without further purification.

The resulting crude thioacetate (0.61 g; 2.11 mmol) was dissolved in anhydrous THF (20 mL; previously degassed) and added dropwise to a stirring slurry of $LiAlH_4$ (0.119 g: 3.12 mmol) at 0 °C. The mixture was allowed to stir at rt for 3 h. The reaction was quenched at 0 °C with H_2O (20 mL; previously degassed) and immediately acidified with 1 M H_2SO_4 (50 mL; previously degassed). The aqueous layer was then extracted with Et_2O (3 × 100 mL), and the organic layer was washed with H_2O (1 × 100 mL) and brine (1 × 100 mL), and dried with $MgSO_4$. Rotary evaporation was used to remove the solvent, and the crude thiol was purified using silica gel chromatography with hexanes as the eluent to give 12,12,13,13,14,14,15,15,16,16,17,17-dodecafluorohenicosane-1-thiol (**H4F6H11SH**) in 91% yield. ^{1}H NMR (500 MHz, $CDCl_3$): δ 2.53 (q, J = 7.45 Hz, 2H), 1.98−2.09 (m, 4H), 1.55−1.63 (m, 6H), 1.28−1.44 (m, 16H), 0.95 (t, J = 7.39 Hz, 3H). ^{19}F NMR (476 MHz, $CDCl_3$): δ −114.3 (m, 4F), −121.8 (m, 4F), −123.6 (m, 4F). ^{13}C NMR (125 MHz, $CDCl_3$): δ 39.2 (s), 34.1 (s), 30.6−31.2 (m), 29.0−29.5 (m), 28.4−28.6 (d), 24.7 (s), 22.2−22.3 (d), 20.2 (s), 13.8 (s), 4.0 (s). Broad peaks at δ 108.9−120.6 are characteristic of a long perfluorocarbon chain.[26] HR-CI-MS, m/z: 543.1969 $[M - H]^+$. Compounds **H5F6H11SH**, **H6F6H11SH**, and **H7F6H11SH** were prepared using an analogous methodology.

*12,12,13,13,14,14,15,15,16,16,17,17-Dodecafluorodocosane-1-thiol (**H5F6H11SH**).* 12,12,13,13,14,14,15,15,16,16,17,17-Dodecafluorodocosane-1-thiol (**H5F6H11SH**) in 85% yield. ^{1}H NMR (600 MHz, $CDCl_3$): δ 2.52 (q, J = 7.33 Hz, 2H), 1.99−2.08 (m, 4H), 1.56−1.62 (m, 6H), 1.28−1.43 (m, 19H), 0.91 (t, J = 7.05 Hz, 3H). ^{19}F NMR (565 MHz, $CDCl_3$): δ −114.5 (m, 4F), −121.9 (m, 4F), −123.7 (m, 4F). ^{13}C NMR (500 MHz, $CDCl_3$): δ 76.8−77.4 (m), 34.1 (s), 31.3 (s), 31.2 (m), 31.0 (m), 30.9 (m), 29.1−29.5 (m), 28.4 (s), 24.7 (s), 22.4 (s), 19.9−20.2 (d), 13.9 (s). Broad peaks at δ 108.7−120.6 are characteristic of a long perfluorocarbon chain.[26] HR-CI-MS, m/z: 557.2106 $[M - H]^+$.

*12,12,13,13,14,14,15,15,16,16,17,17-Dodecafluorotricosane-1-thiol (**H6F6H11SH**).* 12,12,13,13,14,14,15,15,16,16,17,17-Dodecafluorotricosane-1-thiol (**H6F6H11SH**) in 83% yield. ^{1}H NMR (500 MHz, $CDCl_3$): δ 2.53 (q, J = 7.45 Hz, 2H), 1.99−2.09 (m, 4H), 1.56−1.63 (m, 4H), 1.28−1.39 (m, 22H), 1.33 (t, J = 7.73 Hz, 1H), 0.90 (t, J = 6.87 Hz, 3H). ^{19}F NMR (476 MHz, $CDCl_3$): δ −114.3 (m, 4F), −121.8 (m, 4F), −123.6 (m, 4F). ^{13}C NMR (150 MHz, $CDCl_3$): δ 31.5 (s), 31.0 (t, J = 22.8 Hz), 29.1−29.5 (m), 28.9 (s), 28.4 (s), 22.5 (s), 20.2 (s), 14.1 (s). Broad peaks at δ 109.2−120.6 are characteristic of a long perfluorocarbon chain.[26] HR-CI-MS, m/z: 571.2254 $[M - H]^+$.

*12,12,13,13,14,14,15,15,16,16,17,17-Dodecafluorotetracosane-1-thiol (**H7F6H11SH**).* 12,12,13,13,14,14,15,15,16,16,17,17-Dodecafluorotetracosane-1-thiol (**H7F6H11SH**) in 76% yield. ^{1}H NMR (600 MHz, $CDCl_3$): δ 2.53 (q, J = 7.33 Hz, 2H), 1.99−2.08 (m, 4H), 1.55−1.63 (m, 4H), 1.28−1.37 (m, 25H), 0.89 (t, J = 6.87 Hz, 3H). ^{19}F NMR (565 MHz, $CDCl_3$): δ −114.4 (m, 4F), −121.9 (m, 4F), −123.7 (m, 4F). ^{13}C NMR (150 MHz, $CDCl_3$): δ 34.2 (s), 31.7 (s),

DOI: 10.1021/acs.chemmater.9b02887
Chem. Mater. 2020, 32, 953−968

31.1 (t, J = 22.2 Hz), 29.1−29.6 (m), 28.5 (s), 24.8 (s), 22.7 (s), 20.3 (s), 14.2 (s). Broad peaks at δ 109.4−120.5 are characteristic of a long perfluorocarbon chain.[26] HR-CI-MS, m/z: 585.2423 $[M - H]^+$.

Substrate Preparation and Monolayer Formation. Gold slides were prepared by the thermal evaporation of 1000 Å of gold atop 100 Å of chromium on Si(100) wafers under vacuum (pressure $\leq 6 \times 10^{-5}$ Torr) at a rate of 0.5 Å/s. Prior to SAM formation, gold wafers were cut into 3 cm × 1 cm slides, rinsed with absolute ethanol, and dried with ultrapure nitrogen gas. After collecting the ellipsometric constants, two gold slides were immersed per 1 mM thiol solutions (5% THF in EtOH) for 48 h; all solvents were degassed with argon prior to SAM formation. Piranha solution was used to clean the glass vials, which were subsequently rinsed thoroughly with deionized water, followed by absolute ethanol. [**Caution**: Piranha solution is highly corrosive, should never be stored, and should be handled with extreme care.] SAMs were rinsed with THF followed by ethanol and dried using a stream of ultrapure nitrogen gas before characterization.

Characterization of the Monolayers. The thickness values were measured using a Rudolph Research Auto EL III ellipsometer equipped with a He−Ne laser (632.8 nm). The incident angle was set at 70°, and a refractive index of 1.45, typical for an organic film, was used.[36] An average of six measurements (three per slide) was used to obtain the reported thickness.

A PHI 5700 X-ray photoelectron spectrometer was used to obtain the XPS spectra of the SAMs. The instrument was equipped with a monochromatic Al Kα X-ray source (1486.7 eV) incident at 90° relative to the axis of the hemispherical energy analyzer. A take-off angle of 45° from the surface and a pass energy of 23.5 eV were used. The Au $4f_{7/2}$ peak was referenced at a binding energy of 84.0 eV in all of the spectra.

A Nicolet Nexus 670 Fourier transform spectrometer equipped with a mercury−cadmium−telluride detector and a Hinds Instrument PEM-90 photoelastic modulator was used to perform PM-IRRAS. The instrument was set up to allow the p-polarized light to reflect from the surface at an incident angle of 80° with respect to the surface normal. The spectra were collected using 512 scans at a spectral resolution of 2 cm^{-1}.

Vibrational SFG spectroscopy is a surface-sensitive second-order nonlinear spectroscopic technique that under the electric dipole approximation can only give signal at interfaces where the local centrosymmetry of the system is broken.[37] A more detailed explanation of the technique is available in the literature.[37−39] SFG spectroscopy was performed using a pulsed EKSPLA PL-2251A Nd:YAG laser at 1064 nm to pump a LaserVision optical parametric generation/optical parametric amplification (OPG/OPA) system. The OPG/OPA generates the visible 532 nm beam and tunable IR beam in the C−H stretching region from 2750 to 3100 cm^{-1} used in the SFG experiments. The beams, with incident angles of 50° and 60°, respectively, overlap spatially and temporally at the sample surface in a copropagating configuration to generate a new beam with a frequency at the sum of the two input frequencies. The reflected SFG beam is filtered using a monochromator to minimize collinear scattered light from the input 532 nm beam, and is detected using a photomultiplier tube. The resulting spectra were an average of 10 or more scans taken at a scan rate of 1 cm^{-1} s^{-1} with an average of 20 laser shots per data point. Two different polarization combinations, ppp and ssp (for which the letters denote first the SFG, then visible, and then IR beam polarizations with respect to the surface normal), were gathered. Each ppp spectrum was fitted according to the vibrational mode assignments as listed in Table S6 using Mathematica 11 according to eq 1[39]

$$I_{SFG} \propto |\chi_R^{(2)} + \chi_{NR}^{(2)}|^2 = \left| \sum_q \frac{A_q}{\omega_q - \omega_{IR} - i\Gamma_q} + A_{NR} e^{i\varepsilon} \right|^2 \quad (1)$$

where I_{SFG} is the intensity of the SFG signal, $\chi_R^{(2)}$ and $\chi_{NR}^{(2)}$ are the resonant and nonresonant contributions to the second-order nonlinear susceptibility, A_q and Γ_q denote the amplitude and linewidth of the qth vibrational mode at a frequency of ω_q, the infrared frequency is ω_{IR}, A_{NR} and ε are the nonresonant amplitude and phase of the substrate, respectively. The parameters derived from the fitting analysis were used to determine the average orientation (tilt angle) of the methyl group in the FSAMs by using the ratio of the intensities of the symmetric and antisymmetric methyl C−H stretching normal modes compared to a theoretical orientation curve of intensity ratio versus methyl tilt angle as detailed in previous studies.[39−41]

A Ramé-Hart model 100 contact angle goniometer was used to collect the contact angles of the various liquids on the SAM surfaces. A Matrix Technologies micro-Electrapette 25 was used to dispense the liquids at a speed of 1 μL/s. The reported data are an average of 12 measurements, 3 drops per slide from both edges of the drop.

Computational Details. The electronic structure calculations were performed with the ORCA program.[42] The geometries of the partially fluorinated alkanethiols were optimized using the orbital optimized[43] and spin-component-scaled[44] MP2 method in combination with the resolution-of-identity approximation.[45] A double-z basis set (def2-SVP)[46] together with a matching auxiliary basis set def2-SVP/C was applied for all atoms. The optimized geometries of the adsorbates obtained following this method were used to generate a graphical representation of the FSAMs shown in Figure 9.

RESULTS AND DISCUSSION

In this report, the **HnF6H11SH** SAMs were characterized and compared to a series of SAMs derived from their normal alkanethiol analogs (**HmSH**). SAMs derived from normal alkanethiols have been rigorously characterized in several previous studies[24,31,32,36,47,48] and serve here as a reference for the evaluation of the **HnF6H11SH** FSAMs.

Thickness of Monolayers by Ellipsometry. Growth and equilibration of the **HnF6H11SH** adsorbates in gold in EtOH at room temperature yielded SAMs that were thinner than the expected values for similarly structured SAMs, in addition to displaying suboptimal binding of the headgroup to gold and disorder in the alkyl chains.[32] Equilibration of the FSAMs at 40 °C, as in a previous report on similarly structured alkanethiols,[32] led to even more disorder and reduced thicknesses. Consequently, we chose to develop the SAMs in a series of EtOH/THF mixtures in efforts to obtain densely packed and conformationally ordered monolayer films. The thickness measurements obtained for the adsorption of **H2F6H11SH** (chosen as a representative adsorbate) onto gold from various mixtures of solvents are shown in Table S1. It is apparent from the data that high concentrations of THF lead to a reduction of the thickness of the SAMs, and further equilibration at 40 °C failed to yield any significant difference in the thickness values. Additional trials revealed that the FSAMs developed in a mixture of 5% THF and 95% EtOH gave the most densely packed and conformationally ordered monolayers as indicated from analyses by XPS and surface infrared spectroscopy, which are described in following sections.

Given the preceding studies, we generated monolayers from **HnF6H11SH** in a mixture of 5% THF and 95% EtOH with equilibration for 48 h at room temperature. The average thickness values obtained for these FSAMs and the **HmSH** SAMs (developed in EtOH) are displayed in Table 1. Further, the thickness values for the hydrocarbon SAMs gave results that are consistent with the literature.[47] For the SAMs derived from **HnF6H11SH**, however, the average thicknesses were lower than those of their hydrocarbon analogs. In our previous investigation of the first member of this series, **H1F6HnSH**,[32] we attributed such a reduction in thickness to the larger vdW

DOI: 10.1021/acs.chemmater.9b02887
Chem. Mater. 2020, 32, 953−968

Table 1. Ellipsometric Thicknesses of SAMs on Gold Derived from HmSH and HnF6H11SH

adsorbate[a]	thickness (Å)	adsorbate[b]	thickness (Å)
H18SH	23 ± 1	**H1F6H11SH**	17 ± 1
H19SH	25 ± 1	**H2F6H11SH**	18 ± 1
H20SH	26 ± 1	**H3F6H11SH**	19 ± 2
H21SH	27 ± 0	**H4F6H11SH**	18 ± 1
H22SH	28 ± 1	**H5F6H11SH**	21 ± 2
H23SH	31 ± 1	**H6F6H11SH**	22 ± 2
H24SH	32 ± 2	**H7F6H11SH**	22 ± 1

[a]Developed in EtOH. [b]Developed in 95% EtOH and 5% THF.

diameter of the fluorinated segment (~5.6 Å) compared to the smaller hydrocarbon spacer (~4.2 Å) leading to a lower chain density in the films.[4,32] Moreover, the data in Table 1 show that the **HnF6H11SH** FSAMs with the adsorbates having the shortest terminal alkyl chains (methyl, ethyl, propyl, and butyl) all exhibit roughly the same ellipsometric thickness (~18 Å); in contrast, the adsorbates with the longest terminal alkyl chains (pentyl, hexyl, and heptyl) show an initial increase in thickness, which then remains roughly constant (~22 Å). Accordingly, based on the thickness measurements, it appears that the orientation and packing of the molecules in the SAMs depend, at least in part, on the length of the terminal alkyl chain.

Composition and Packing of Monolayers by XPS. The XPS spectra of the C 1s and S 2p photoelectrons for the **HmSH** SAMs are presented in Figure 3, and their binding

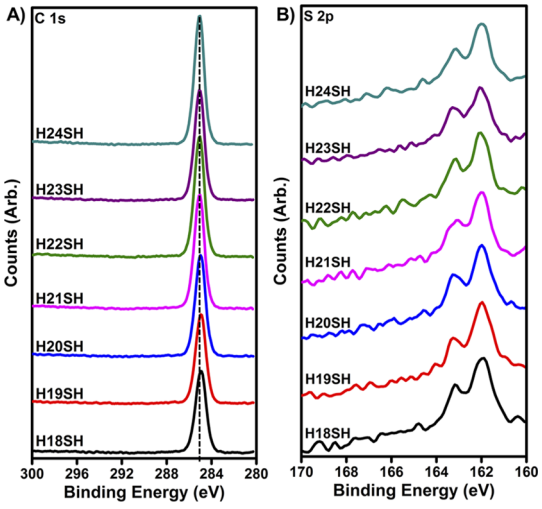

Figure 3. XPS spectra of the (A) C 1s and (B) S 2p regions collected from the **HmSH** SAMs.

energies as well as percentage of bound sulfur are listed in Table S2. The spectra for all of the **HmSH** SAMs exhibit a characteristic doublet in the S 2p region in a 1:2 ratio, which is assigned to the S $2p_{3/2}$ and S $2p_{1/2}$ electrons.[49,50] For a thiolate bound to gold, the S $2p_{3/2}$ peak is characterized by a binding energy of ~162 eV; moreover, the absence of peaks at ~164 and ~168 eV indicates that there are no unbound or oxidized sulfur species, respectively, in the samples.[49,50] Additionally, we calculate the percentage of bound thiolates (Table S2) by deconvoluting the S 2p peaks, shown in Figure S19. The XPS data presented here can therefore be taken to indicate that the sulfur atoms in all of these monolayers are mostly bound (98, 93, 92, 89, 91, 91, and 88% for **H18SH**, **H19SH**, **H220SH**, **H21SH**, **H22SH**, **H23SH**, and **H24SH**, respectively) to gold as surface thiolates. We note also that the absence of any peaks for fluorine is consistent with the chemical makeup of the all-hydrocarbon **HmSH** adsorbates.

The C 1s, F 1s, and S 2p regions for the **HnF6H11SH** FSAMs are presented in Figure 4, and their corresponding binding energies and percentage of bound sulfur are listed in Table S3. Deconvolution of the S 2p peaks for the **HnF6H11SH** FSAMs (Figure S20) reveals that the monolayers are mostly bound: 82, 83, 81, 91, 93, 96, and 88% for **H1F6H11SH**, **H2F6H11SH**, **H3F6H11SH**, **H4F6H11SH**, **H5F6H11SH**, **H6F6H11SH**, and **H7F6H11SH**, respectively. The C 1s region of the **HnF6H11SH** FSAMs in Figure 4A shows two peaks at ~284 and ~291 eV that are associated with the CH_2 and CF_2 carbons, respectively.[32] Analysis of the binding energies of the C 1s photoelectrons arising from the CH_2 carbons can give insight into the relative packing density of the film; typically, an increase in the binding energy of the peak indicates an increase in the packing density of the alkyl spacer in the SAMs.[36,51,52] Examination of the peak position of the C 1s (CH_3/CH_2) for the **HnF6H11SH** FSAMs reveals a shift to higher binding energies as the top alkyl chain is extended. For the SAMs with the longer alkyl chains (i.e., **H5F6H11SH** and longer), the FSAMs appear to pack similarly to the hydrocarbon SAMs, with a binding energy of ~285.0 eV. Additionally, examination of the peak position of the F 1s electrons shows that as the length of the terminal alkyl chain is increased, the binding energy decreases; notably, an analogous shift is observed in the binding energy of the C 1s electrons of the CF_2 moieties. Previous reports have observed a similar shift for the binding energy of the fluorinated segments for FSAMs in which the underlying spacer is systematically increased.[30] Such an effect has been attributed to the greater distance between the gold substrate and the excited atoms.[30,36,53] As, however, the distance between the gold substrate and the fluorinated segments in the **HnF6H11SH** SAMs is constant, a different phenomenon must be causing the shifts observed here.

The CH_2 C 1s binding energies for the FSAMs derived from adsorbates having terminal methyl and ethyl groups (BE = 284.5−284.6 eV associated with loose packing) seem to indicate that the vdW and steric interactions between the fluorinated segments strongly influence the structure/packing of these SAMs; in contrast, the CH_2 C 1s binding energies for the FSAMs derived from the adsorbates having terminal propyl, butyl, pentyl, hexyl, and heptyl chains (BE = 284.8−285.0 eV associated with dense "crystalline" packing) suggest that the alkyl chains as a whole control the structure/packing of these latter SAMs. In Table S3, given that the shifts in the F 1s and CF_2 C 1s binding energies as the length of the terminal alkyl is increased behave oppositely to the corresponding shifts in the CH_2 C 1s binding energies, we interpret the shifts observed here to indicate that loose packing is induced in the fluorinated segments as the length of the terminal alkyl chains is increased. As per variation in the molecular density of the SAMs because of different chain lengths, Tables S4 and S5 indicate that all of the monolayers within the series have similar densities.

In addition to the shifts in the binding energies of the electrons of the **HnF6H11SH** FSAMs, the shape of the peak associated with the C 1s (CH_2/CH_3) provides additional information. There is an asymmetry and/or broadening

DOI: 10.1021/acs.chemmater.9b02887
Chem. Mater. 2020, 32, 953−968

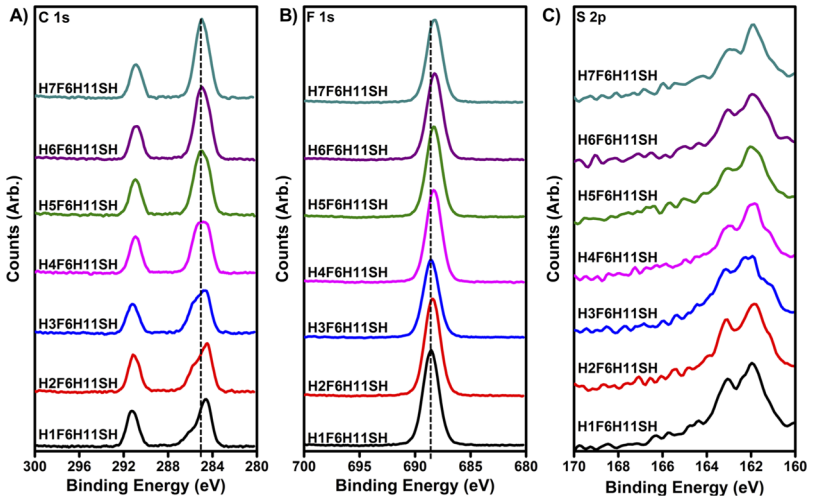

Figure 4. XPS spectra of the (A) C 1s, (B) F 1s, and (C) S 2p regions collected from the **HnF6H11SH** SAMs.

associated with the **HnF6H11SH** FSAMs where n = 1−4, which perhaps arises from the impact of the perfluorocarbons on the binding energies of the adjacent CH_2 species. For the films with the longer terminal alkyl chains, however, it is plausible that the signal intensities from those photoelectrons are attenuated.

Conformational Order of Monolayers by PM-IRRAS. We utilized PM-IRRAS to obtain insight into the packing/orientation of the terminal group in the FSAMs as well as the relative conformation of the alkyl chains. Figure 5 shows the PM-IRRAS spectra for the C−H stretching vibration region for the hydrocarbon SAMs and **HnF6H11SH** FSAMs examined in this study, and the peak positions are listed in Table S6. The C−F stretching regions of the **HnF6H11SH** FSAMs were also examined and are shown in Figure S22. However, there was no discernible difference between the spectra; therefore, the focus of our analysis will be on the C−H stretching region. Previous research has utilized the position of the methylene C−H antisymmetric stretching vibration as an indicator of the relative conformational order of the films; specifically for a well-ordered highly crystalline film, the antisymmetric vibration ($\nu_{as}^{CH_2}$) appears at ∼2918 cm^{-1}.[36,54,55] Conversely, a shift to higher wavenumbers is an indication of a disordered film. All of the SAMs examined in this study exhibit a $\nu_{as}^{CH_2}$ of 2918 ± 2 cm^{-1}, indicating well-ordered SAMs with the hydrocarbon chains having mostly trans-extended conformations.[36,54,55]

The position of the antisymmetric C−H stretching vibration associated with the methyl, $\nu_{as}^{CH_3}$, provides additional insight into the structure of these SAMs. For the SAM derived from **H1F6H11SH**, the peak associated with $\nu_{as}^{CH_3}$ is hardly visible in the IR because of the diminution of the $\nu_{as}^{CH_3}$ peaks by the adjacent fluorocarbon segment.[32,56] For the SAM derived from **H2F6H11SH**, we would expect the $\nu_{as}^{CH_3}$ peak to appear at ∼2985 cm^{-1}, in agreement with the bulk IR and Raman spectra for this molecule (Figure S21) as well as model compounds found in the literature.[56] However, this peak is not visible in the PM-IRRAS spectrum possibly because of the orientation of the methyl group (as detailed below in the SFG section) and/or the proximity of the methyl group to the perfluorocarbon segment.[32,56] In contrast, the $\nu_{as}^{CH_3}$ peak for the SAM derived from **H3F6H11SH** appears at 2977 cm^{-1}, and this peak shifts to lower frequencies as the terminal alkyl chain is lengthened, plateauing for the butyl, pentyl, hexyl, and heptyl analogs at a value similar to that observed for SAMs derived from alkanethiols (∼2964 cm^{-1}). A similar trend is observed for the symmetric CH_3 stretch ($\nu_{s}^{CH_3}$). Notably, this trend mirrors that found in the peak positions of the methyl carbon in the carbon NMR data of the corresponding adsorbates, with the exception of the **H2F6H11SH** (see Figure S23 and Table S7). We are currently undertaking additional studies to determine the origin of the shifts highlighted here.

In addition to the conformational order of the SAMs and the shifts observed for the methyl vibrations, the relative intensity of the $\nu_{as}^{CH_3}$ and $\nu_{s}^{CH_3}$ peaks for the SAMs can yield some insight into the orientation of the terminal methyl group. In the surface IR spectra of the hydrocarbon SAMs, there is a variation in the relative intensity of the vibrations associated with the methyl group that depends on the total number of carbons in the chain. For the chains having an even number of carbon atoms (**HmSH**, where m = 18, 20, 22, and 24), the ratio of the intensity of $\nu_{s}^{CH_3}$ to $\nu_{as}^{CH_3}$ is ∼1:1, whereas for the chains having an odd number of carbon atoms, (**HmSH**, where m = 19, 21, and 23), the ratio is ∼1:2. Odd−even effects have been observed in the surface IR spectra of hydrocarbon SAMs generated from n-alkanethiols on gold and have been attributed to the change in direction of the transition dipole moment (TDM) of the vibration as the structure of the SAM changes with the total number of carbons in the chain, thereby altering its IR intensity according to the metal surface selection rule that governs surface IR techniques.[51,57]

The spectra of the **HnF6H11SH** FSAMs having terminal alkyl chains longer than two carbon atoms (**HnF6H11SH**, where n = 3−7) also show a variation in the intensity of the C−H stretches of the methyl groups (see Figure 5). In the FSAM series, the odd−even trend is opposite to that observed in the corresponding hydrocarbon SAMs and varies alternately with the number of carbons in the terminal alkyl chain. In this case, the films with odd-numbered chains have a high $\nu_{s}^{CH_3}$ to $\nu_{as}^{CH_3}$ ratio of ∼1:1, and the films with even-numbered chains have a lower ratio of ∼1:2 (see Figure 5). Considering the reversal of the odd−even effect in the **HnF6H11SH** FSAMs and the IR surface selection rules for films on metal surfaces,

DOI: 10.1021/acs.chemmater.9b02887
Chem. Mater. 2020, 32, 953−968

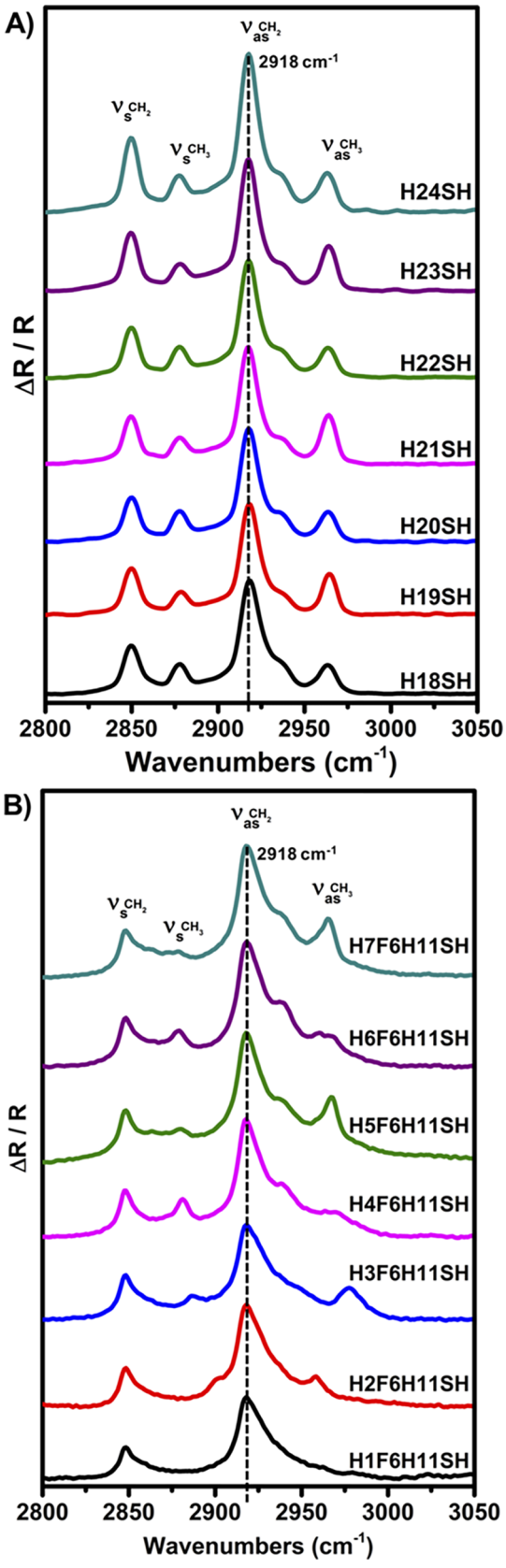

Figure 5. PM-IRRAS spectra for the C−H stretching region collected from (A) **HmSH** SAMs and (B) **HnF6H11SH** FSAMs.

we can conclude that, with respect to total chain length, the terminal methyl groups are oriented oppositely for the **HnF6H11SH** SAMs compared to the **HmSH** SAMs.

Based on the metal surface selection rules, components of the TDM that are perpendicular to the surface can be strongly excited by the p-polarized radiation (with respect to the surface normal) used in surface infrared spectroscopy and thereby are easily detected, whereas those parallel to the surface will be too weakly excited to produce detectable signal.[58] Following these guidelines, we can conclude that the methyl group in **HnF6H11SH** FSAMs with even-numbered chain lengths (**HnF6H11SH** where n = 3, 5, and 7) must be tilted away from the surface normal. In this scenario, the TDM of the antisymmetric stretch is pointed somewhat perpendicular to the gold surface, causing both peaks ($\nu_s^{CH_3}$ and $\nu_{as}^{CH_3}$) to have similar intensity. On the other hand, in the **HnF6H11SH** FSAMs with odd-numbered chain lengths (**HnF6H11SH** where n = 4 and 6), the TDM for the symmetric stretch is more closely aligned with the surface normal, and for the antisymmetric stretch, it is tilted away from the surface normal, causing $\nu_s^{CH_3}$ to be more intense than $\nu_{as}^{CH_3}$. A quantitative analysis of the orientation of the terminal methyl group is discussed in the following SFG section.

Orientation of the Methyl Group by SFG. We employed SFG spectroscopy to determine the orientation of the terminal methyl group and gain insight into the effect of fine shifts in structure on the physical properties of the films. In contrast to the PM-IRRAS spectra above, the $\nu_{as}^{CH_3}$ peak is visible in the SFG spectra because of the interface-selectivity of the technique.[37] The normalized and fitted SFG spectra of the C−H stretching region for the **HnF6H11SH** FSAMs are presented in Figure 6, where the symmetric, $\nu_s^{CH_3}$, antisymmetric, $\nu_{as}^{CH_3}$, and fermi resonance, $\nu_{FR}^{CH_3}$, methyl C−H stretching peak positions are marked with gray dotted lines and the symmetric, $\nu_s^{CH_2}$, and antisymmetric, $\nu_{as}^{CH_2}$ methylene C−H stretching peak positions are marked with black dotted lines. Additional discussion regarding peak assignment can be found in the Supporting Information. The SFG spectrum of the **H18SH** SAM is also shown for comparison of stretching frequencies and relative peak intensities. All peak intensities in the SFG spectra were fit according to Lorentzian line shapes following the peak assignments listed in Table S6. The fitting parameters and intensity ratios used in the determination of the orientation of the methyl group are listed in Table S8.

Apparent from Figure 6 and Table S6, proximity to the fluorinated chain dramatically blue-shifts the methyl group $\nu_s^{CH_3}$ and $\nu_{as}^{CH_3}$ stretching frequencies for films with short alkyl chains (**HnF6H11SH**, where n = 1−3), whereas the films with longer alkyl chains (**HnF6H11SH**, where n = 4−7) show similar peak positions to films derived from *n*-alkanethiols (i.e., **H18SH**). These spectra, together with the PM-IRRAS and XPS, demonstrate that the effect of the fluorocarbons diminishes after three CH_2 groups separate the methyl group and the fluorinated segment. Similarly, a study by Laibinis et al. found that the influence of an embedded oxygen atom in an alkanethiol SAM on the stretching frequencies of a methyl group diminished by extending the distance between the oxygen and the methyl group by three methylene groups.[59]

To gain a better understanding of the monolayer structure, we determined the orientation of the terminal methyl group in these SAMs using the ratio of SFG peak intensities from the

DOI: 10.1021/acs.chemmater.9b02887
Chem. Mater. 2020, 32, 953−968

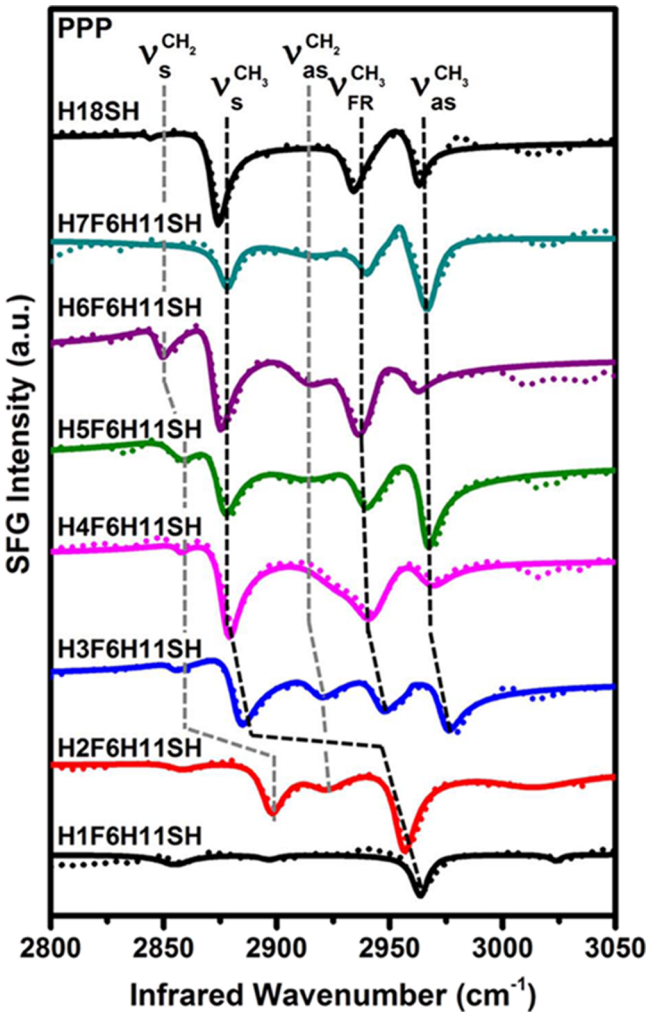

Figure 6. Normalized SFG spectra for the C−H stretching region collected from **HnF6H11SH** FSAMs. The solid lines denote the fits to the spectra according to eq 1. PPP denotes the polarization direction of the SFG, visible, and IR beams, in that order, with respect to the surface normal. The symmetric, $\nu_s^{CH_3}$, and antisymmetric, $\nu_{as}^{CH_3}$, methyl C−H stretching peak positions are marked with black dotted lines. The SFG spectrum of **H18SH** is included as a reference.

symmetric and antisymmetric methyl C−H stretches in the ppp spectra.[38,60] Note, assignment of the methyl stretches used in this analysis is detailed in the Supporting Information. Based on this analysis, the average tilt angle along the terminal C−C bond of the methyl group with respect to the surface normal, hereafter described as the "methyl group tilt angle," was determined for each **HnF6H11SH** FSAM, and the results are plotted in Figure 7. The data assume a delta distribution of orientation angles, and the asymmetric error bars indicate a possible range of methyl group tilt angles derived from the simulated orientation curve (Figure S24) based on the error in the intensity ratios.

Figure 7 shows a clear odd−even effect in the orientation of the terminal methyl group, where films with even-numbered chains (**HnF6H11SH**, where n = 1, 3, 5, and 7) show a methyl group tilt angle more parallel to the surface than the films with odd-numbered chains (**HnF6H11SH**, where n = 2, 4, and 6). This result is consistent with the qualitative observations from the PM-IRRAS spectra, given that an upright tilt angle for the final C−C bond in the molecule causes the even-numbered

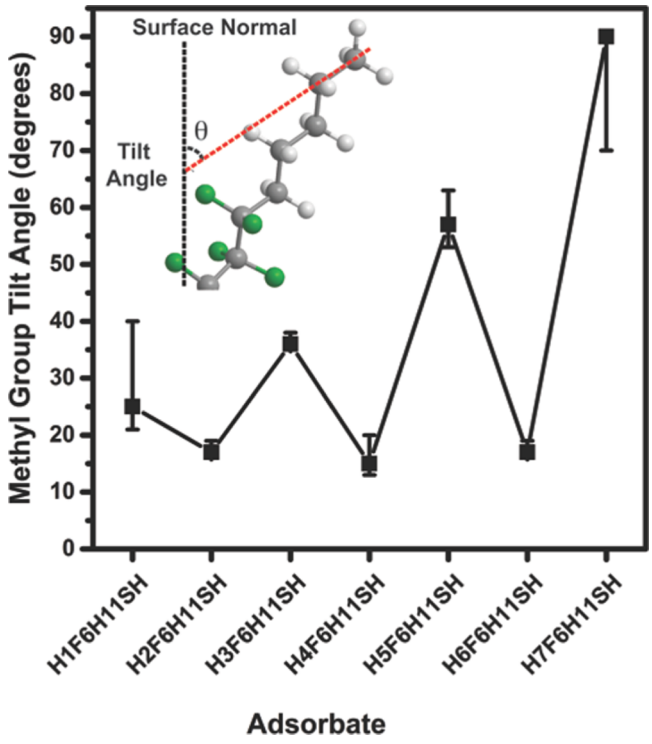

Figure 7. Average methyl group tilt angle of the **HnF6H11SH** FSAMs, derived from the SFG spectra. The figure in the corner is a pictorial representation of the methyl group tilt angle and is not meant to indicate that the chain underneath the methyl group will follow the same tilt angle. Small error bars lie within the symbol.

chains to exhibit strong $\nu_{as}^{CH_3}$ peak intensities, whereas those of the odd-numbered chain are weak. Because of the distance between the methyl group and the fluorocarbon segment, the $\nu_{as}^{CH_3}$ is visible in the PM-IRRAS spectra of the **H4F6H11SH** and **H6F6H11SH** adsorbates, despite their upright orientation. Additionally, the odd−even effect observed in the orientation of the methyl group in the FSAMs corresponds to what has been observed in *n*-alkanethiol SAMs having the same total carbon count as the top alkyl segment of the **HnF6H11SH** adsorbates (i.e., the same as SAMs on Au(111) derived from **HmSH**)[61] and is due to the overall tilted structure of the carbon backbone on the gold surface.[36,48,59]

Finally, the appearance of strong methylene contributions with resonances at ∼2850 and ∼2920 cm^{-1} in the SFG spectra of both allowed polarization combinations, ppp (Figure 6) and ssp (Figure S25), lends evidence to the relative disorder of the top-most alkyl chains in the FSAMs compared to a pure hydrocarbon SAM (**H18SH**), also corroborating the analysis by XPS. The short chain above the spatially larger fluorinated segment is plausibly conformationally disordered, leading to the top-most alkyl segment of the **HnF6H11SH** FSAMs to adopt similar packing behavior to that of short *n*-alkanethiol SAMs (i.e., **H7SH**) on Au.[36] Hydrocarbon SAMs that are loosely packed and disorganized have gauche defects that break the local centrosymmetry of the methylene groups in an otherwise trans-extended chain, giving rise to the SFG signal.[37] The presence of peaks associated with the methylene groups and the terminal group orientation analysis performed further demonstrate that the terminal groups of the **HnF6H11SH** FSAMs are orientationally similar to that of regular alkanethiols with the same overall length as the alkylated

DOI: 10.1021/acs.chemmater.9b02887
Chem. Mater. 2020, 32, 953−968

segment (i.e., **HmSH** where $n = m$). However, these groups exhibit blue-shifted stretching frequencies plausibly because of their interaction with the electron-withdrawing fluorinated segments.

Interfacial Properties by Contact Angles. The interfacial energy and heterogeneity of a film can be determined by examining the wetting behavior of the film when exposed to a systematically chosen set of contacting probe liquids. Recently,[12] we evaluated the impact of the inverted HC−FC dipole (representing the hydrocarbon−fluorocarbon junction) and the "normal" FC−HC dipole (representing the fluorocarbon−hydrocarbon junction) on the transport properties of SAMs on gold. In the present study, we used several polar and nonpolar liquids to probe the influence of the HC−FC dipole as it was buried in the **HnF6H11SH** FSAMs.

We used the nonpolar liquids decalin (DC), hexadecane (HD), and the weakly polar bromonaphthalene (BNP) along with the fluorocarbon liquid perfluorodecalin (PFD) to probe the dispersive interactions. The polar liquids used included a series of polar aprotic liquids of varying polarity: nitrobenzene (NB), dimethylsulfoxide (DMSO), dimethylformamide (DMF), and acetonitrile (ACN). Additionally, we used three polar protic liquids: water (H_2O), formamide (FA), and glycerol (GL). For the sake of comparison, we also examined the wettability of the SAMs derived from the corresponding *n*-alkanethiols.

Probing Dispersive Interactions with the Nonpolar Liquids. Figure 8 and Table S9 show the advancing contact angles obtained for the nonpolar liquids on the SAMs. In Figure 8A, there is a clear odd−even effect in the wettability data of the **HmSH** SAMs in which the odd SAMs are more wettable than the even SAMs, an observation that agrees with literature studies of alkanethiols on Au.[32,48,62] In contrast, for the **HnF6H11SH** FSAMs (Figure 8B), the contact angles of the nonpolar liquids DC and HD systematically decrease as the length of the terminal alkyl chain is increased until the values reach those of the hydrocarbon SAMs. For the **HnF6H11SH** FSAMs having $n = 1-3$, there appear to be unfavorable dispersive interactions between the contacting liquids and the underlying fluorinated segment, leading to an increase in the contact angles compared to the hydrocarbon SAMs. For the **HnF6H11SH** FSAMs having $n = 4-7$, no unfavorable interactions between the contacting liquid and the fluorinated segment can be detected, in accordance with the observations made from the XPS, PM-IRRAS, and SFG spectra.

Additionally, an odd−even effect can be seen for the **HnF6H11SH** FSAMs having $n = 4-7$ in which the SAMs with a top alkyl chain length having an odd number of carbon atoms are more wettable than those having an even number of carbon atoms. In the former SAMs, the terminal methyl group is tilted away from the surface normal, as described in the SFG section, exposing the underlying CH_2 groups and increasing molecular contact between the surface and the liquid,[32,48,62] as depicted in Figure 9.

The wettability of PFD on the **HnF6H11SH** FSAMs (see Figure 8B) offers additional insight regarding the effect of the underlying fluorocarbon segment on the wettability of these SAMs. The contact angles of the PFD on the **HnF6H11SH** FSAMs where $n = 1-3$ imply that the fluorocarbon moieties are exposed at the interface of these SAMs, possibly because of the short length of the top chain leading to a loosely packed state that allows for penetration of the liquid further into the film compared to a densely packed monolayer. The contact angle of PFD on the **H2F6H11SH** SAM is dramatically higher than that for the **H1F6H11SH** SAM because of unfavorable interactions between the fluorinated liquid and the hydrocarbon interface. However, there is a slight decrease in the contact angle on the **H3F6H11SH** surface, which could be due to the ethyl group being pointed more upright on the surface, whereas the propyl group is more tilted away, exposing the CF_2 at the interface. Another dramatic increase in the contact angle is observed upon going from the propyl- to butyl-terminated FSAM, an odd−even effect greatly affected by the underlying CF_2. For the **HnF6H11SH** FSAMs with $n = 4-7$, the odd−even effect continues to be observed, but it is less substantial than that for the **HnF6H11SH** FSAMs with $n = 1-3$. Finally, the bulky aromatic BNP is the outlier here: on the **HnF6H11SH** FSAMs, the contact angles of BNP are roughly the same across the series. The size and planar geometry of the liquid might be responsible for the observed invariance.

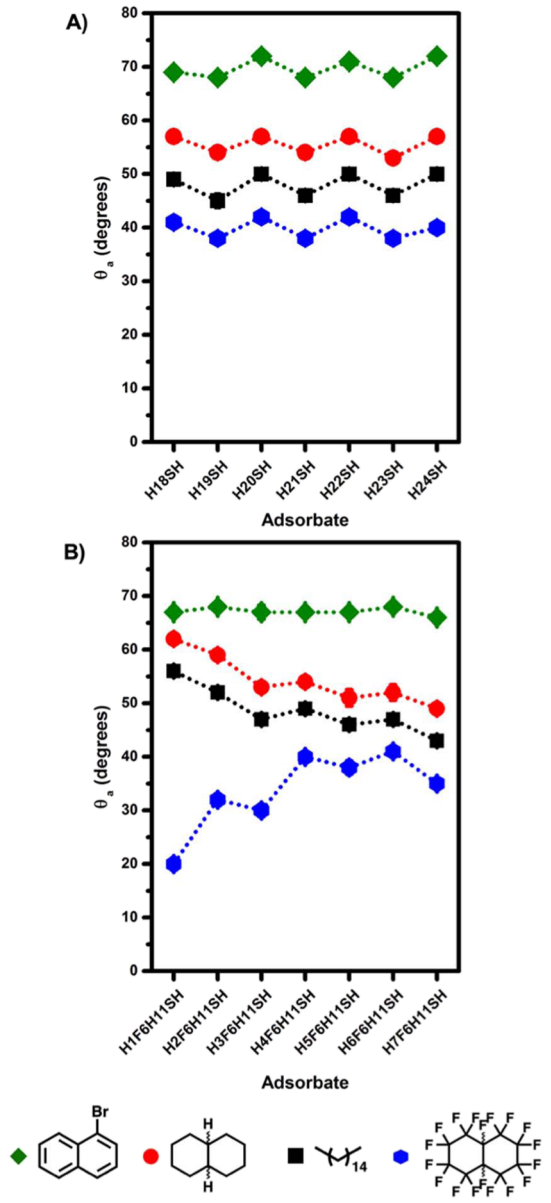

Figure 8. Advancing contact angle values of the nonpolar liquids on (A) **HmSH** SAMs and (B) **HnF6H11SH** FSAMs. Small error bars lie within the symbol.

DOI: 10.1021/acs.chemmater.9b02887
Chem. Mater. 2020, 32, 953−968

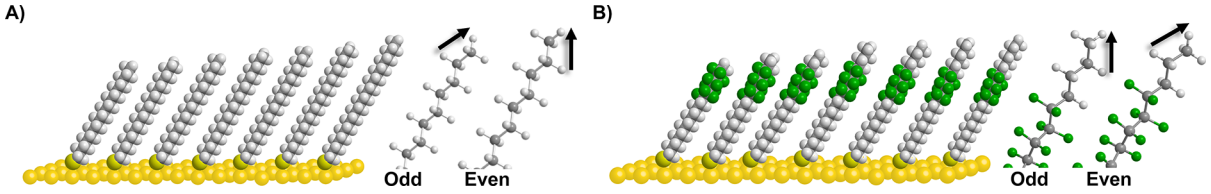

Figure 9. Depiction of the terminal methyl group orientation in the SAMs derived from the adsorption of (A) **HmSH** and (B) **HnF6H11SH** SAMs on gold. Details of the molecular modeling of the adsorbates are described in the Experimental Section.

Probing the Effect of the HC−FC Dipole with Polar Aprotic Liquids. To gain further insight into the interfacial properties of the films (including the potential impact of the HC−FC dipole), the SAMs were probed with a variety of polar aprotic and protic liquids of varying polarity. Figure 10 shows the advancing contact angles of the polar aprotic liquids DMSO, DMF, ACN, and NB on the SAMs (see also Table S10). For the hydrocarbon **HmSH** SAMs (Figure 10A), the contact angles exhibit an apparent odd−even effect in which the odd SAMs are more wettable than the even SAMs, consistent with the trends observed with the nonpolar liquids in Figure 8A. However, for the **HnF6H11SH** FSAMs (Figure 10B), there is a systematic increase in the contact angles of the polar aprotic liquids, with the exception of NB (vide infra); this trend is consistent with a model in which the HC−FC is buried into the film as the length of the alkyl chain is increased. More specifically, as the length of the alkyl chain is extended, the distance-dependent dipole−dipole interactions (Keesom forces) between the HC−FC dipoles and those of the contacting liquid become weaker, which gives rise to increasing contact angle values.

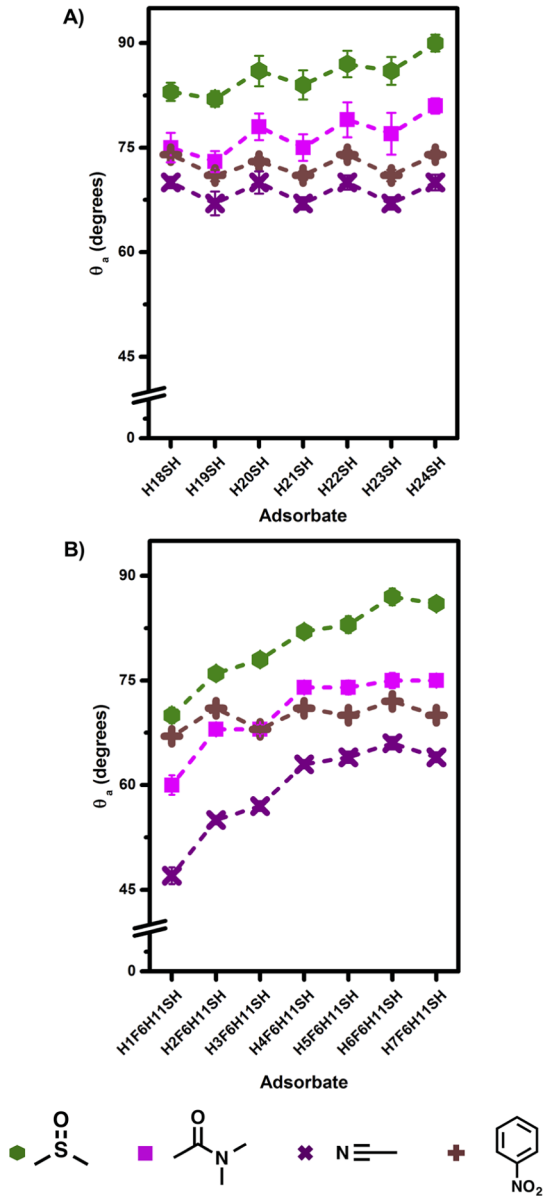

Figure 10. Advancing contact angle values of the polar aprotic liquids on the (A) **HmSH** SAMs and (B) **HnF6HnSH** FSAMs. Small error bars lie within the symbol.

We note also that the polar aprotic contacting liquids fail to exhibit a clear odd−even effect on the **HnF6H11SH** FSAMs, save for NB, where the contact angles vary systematically with the length of the terminal alkyl chain. The lack of an odd−even effect for DMSO, DMF, and ACN is likely due to intercalation of these relatively small molecules into the slightly disordered top alkyl portion of the **HnF6H11SH** FSAMs, as described in the SFG section, as well as the strong dipole of these liquids (DMSO = 3.96 D; DMF = 3.86 D; and ACN = 3.20 D).[63,64] It is further interesting to note that the **HnF6H11SH** FSAMs where n is odd (**H1F6H11SH**, **H3F6H11SH**, **H5F6H11SH**, and **H7F6H11SH**) are more wettable by the sterically larger NB than the **HnF6H11SH** FSAMs where n is even (**H2F6H11SH**, **H4F6H11SH**, **H6F6H11SH**). Furthermore, the odd−even effect is opposite to that observed on the hydrocarbon **HmSH** SAMs of corresponding overall chain length, an observation that is reinforced by the analysis made in the IR and SFG sections above regarding the orientation of the terminal methyl group. Although the orientation of the terminal methyl moiety plays a role in the wettability of the NB, the effect of the HC−FC dipole for the shorter alkyl chains also contributes to the wetting properties of the films (for NB, μ = 4.22 D).[63,64] The difference in the contact angle for the **H1F6H11SH** SAM (67°) and the **H2F6H11SH** SAM (71°) is greater than that for the contact angles of the **H4F6H11SH** SAM (71°) and the **H5F6H11SH** SAM (70°), suggesting a greater dipole−dipole interaction between the HC−FC dipole and the dipole of the NB contacting liquid for the shorter alkyl chains.

Role of H-Bonding in Polar Protic Liquids on the Wettability of the FSAMs. We also probed the SAMs with various polar protic liquids (Figure 11). The contact angle data in Figure 11A on the **HmSH** SAMs show comparable values and no strong odd−even effects as observed in previous studies of SAMs on gold derived from *n*-alkanethiols.[31,32,62] Notably, our previous study of SAMs derived from the **H1F6HnSH** series found not only odd−even effects for polar protic liquids, but also a reversal in the odd−even trend of polar protic liquids compared to polar aprotic liquids on these SAMs.[32] The

DOI: 10.1021/acs.chemmater.9b02887
Chem. Mater. 2020, 32, 953−968

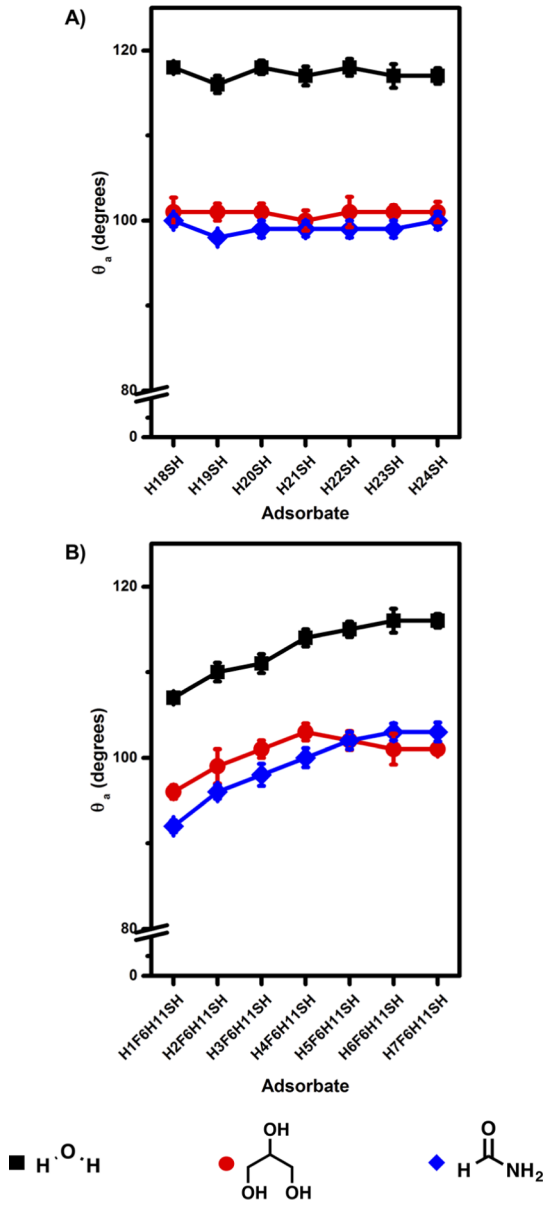

Figure 11. Advancing contact angle values of the polar protic liquids on the (A) **HmSH** SAMs and (B) **HnF6HnSH** FSAMs. Small error bars lie within the symbol.

reversal was attributed to the unfavorable interaction between the dipoles of the FSAM surface and the polar protic contacting liquids (i.e., δ^+ at the SAM interface and δ^+ of the contacting liquids) as well as the inability of the contacting liquids to undergo favorable interfacial rearrangement/orientation because of their extensive H-bonding network.[32] However, in the present study of polar protic liquids on the **HnF6H11SH** FSAMs (Figure 11B), we observe no obvious odd−even effects and thus no corresponding trend reversal. Similar to the aprotic liquids, the contact angles of the polar protic liquids (H_2O, GL, and FA) on the **HnF6H11SH** FSAMs increase as the length of the terminal alkyl chain is increased, until reaching values similar to those found on the hydrocarbon **HmSH** SAMs. The decreasing trend in wettability (i.e., higher contact angles) of these liquids further supports a model in which the influence of the HC−FC dipole weakens as the dipole is systematically buried into the film, as observed with the aprotic liquids (vide supra). Furthermore, the weakness of the buried dipoles limits their possible impact on any odd−even trends in wettability.

Interestingly, our previous studies of FC−HC dipole-based films found that increasing the amount of terminal fluorination led to decreases in wettability for both polar and nonpolar contacting liquids,[28,29] which is consistent with a model in which the FC−HC dipole is buried. In contrast, the inverted HC−FC dipole-based films described here showed a decrease in wettability for polar liquids but an increase in wettability for nonpolar liquids as the HC−FC dipole was buried. These differing trends no doubt arise from the weak attractive forces between the former fluorocarbon-terminated FC−HC films and the nonpolar hydrocarbon-based probe liquids, which interact more strongly with the latter hydrocarbon-terminated HC−FC films.

Overall, the data presented here collectively suggest that the orientation of the terminal methyl group in the **HnF6H11SH** FSAMs is opposite to that of the hydrocarbon SAMs of a corresponding chain length, suggesting that the fluorinated segment behaves as a surrogate surface from which the top hydrocarbon segment builds until the interfacial properties match those of short-chain *n*-alkanethiol-based SAMs on gold.

CONCLUSIONS

A new series of alkyl-terminated fluorinated alkanethiols was synthesized and used to generate FSAMs on gold. Analysis by ellipsometry found that there were no significant differences in the thicknesses of the **HnF6H11SH** FSAMS with n = 1−4 (∼18 Å) and similarly for **HnF6H11SH** FSAMS with n = 5−7 (∼21 Å). We also found that the nature of the adsorbate (i.e., the differences in the vdW diameter of the hydrocarbon and fluorocarbon segments, the helical nature of the fluorocarbon segment, and the location of the HC−FC dipole) exhibits a profound effect on the interfacial properties of the films. Analysis by XPS revealed an increase in the packing density of the hydrocarbon segments as the terminal alkyl chain length was increased with a concomitant reduction in the packing density of the fluorocarbon segments. Analysis using surface IR found that all of the **HnF6H11SH** FSAMs were well-ordered. Furthermore, an odd−even effect was observed for the methyl C−H stretching bands that corresponded to the number of carbons in the terminal alkyl chain rather than the total number of carbons. This observation suggests that the fluorocarbon segment behaves as a surrogate surface in which the odd−even effect follows the trend for short-chain *n*-alkanethiol-based SAMs on gold. This finding was validated by SFG methyl group orientation analysis, which showed a systematic change in the tilt angle of the terminal C−C bond with odd−even variations in the length of the terminal alkyl group. Correspondingly, the wettability data were strongly influenced by the orientation of the terminal methyl groups in these types of SAMs. As per the interfacial energies of these monolayers, the contact angle data showed that the underlying HC−FC dipoles and the structure of the adsorbate have a strong effect on the wettability of the monolayer, with the influence of the HC−FC surface dipole dissipating as the length of the terminal alkyl group is increased (i.e., as the dipole is buried into the film).

DOI: 10.1021/acs.chemmater.9b02887
Chem. Mater. 2020, 32, 953−968

■ ASSOCIATED CONTENT

Supporting Information

The Supporting Information is available free of charge at https://pubs.acs.org/doi/10.1021/acs.chemmater.9b02887.

Details on NMR characterization of the adsorbates (^{1}H, ^{19}F, and ^{13}C), additional ellipsometry data, additional XPS data, additional surface IR data, IR and Raman spectra of the bulk adsorbates, background information for the SFG analysis, and detailed contact angle data (PDF)

■ AUTHOR INFORMATION

Corresponding Author

*E-mail: trlee@uh.edu.

ORCID

Tianlang Yu: 0000-0001-6218-5694

Steven Baldelli: 0000-0002-5747-259X

T. Randall Lee: 0000-0001-9584-8861

Notes

The authors declare no competing financial interest.

■ ACKNOWLEDGMENTS

The authors are grateful for financial support from the National Science Foundation (CHE-1710561), the Robert A. Welch Foundation (E-1320), and the Texas Center for Superconductivity.

■ REFERENCES

(1) Srinivasan, U.; Houston, M. R.; Howe, R. T.; Maboudian, R. Alkyltrichlorosilane-Based Self-Assembled Monolayer Films for Stiction Reduction in Silicon Micromachines. *J. Microelectromech. Syst.* **1998**, *7*, 252−260.

(2) Palacio, M.; Bhushan, B. Ultrathin Wear-Resistant Ionic Liquid Films for Novel MEMS/NEMS Applications. *Adv. Mater.* **2008**, *20*, 1194−1198.

(3) Pujari, S. P.; Spruijt, E.; Cohen Stuart, M. A.; van Rijn, C. J. M.; Paulusse, J. M. J.; Zuilhof, H. Ultralow Adhesion and Friction of Fluoro-Hydro Alkyne-Derived Self-Assembled Monolayers on H-Terminated Si(111). *Langmuir* **2012**, *28*, 17690−17700.

(4) Zenasni, O.; Jamison, A. C.; Lee, T. R. The Impact of Fluorination on the Structure and Properties of Self-Assembled Monolayer Films. *Soft Matter* **2013**, *9*, 6356−6370.

(5) Fréchette, J.; Maboudian, R.; Carraro, C. Thermal Behavior of Perfluoroalkylsiloxane Monolayers on the Oxidized Si(100) Surface. *Langmuir* **2006**, *22*, 2726−2730.

(6) Hoque, E.; DeRose, J. A.; Hoffmann, P.; Mathieu, H. J. Robust Perfluorosilanized Copper Surfaces. *Surf. Interface Anal.* **2006**, *38*, 62−68.

(7) Pujari, S. P.; Scheres, L.; Weidner, T.; Baio, J. E.; Cohen Stuart, M. A.; van Rijn, C. J. M.; Zuilhof, H. Covalently Attached Organic Monolayers onto Silicon Carbide from 1-Alkynes: Molecular Structure and Tribological Properties. *Langmuir* **2013**, *29*, 4019−4031.

(8) Ma, H.; Yip, H.-L.; Huang, F.; Jen, A. K.-Y. Interface Engineering for Organic Electronics. *Adv. Funct. Mater.* **2010**, *20*, 1371−1388.

(9) de Boer, B.; Hadipour, A.; Mandoc, M. M.; van Woudenbergh, T.; Blom, P. W. M. Tuning of Metal Work Functions with Self-Assembled Monolayers. *Adv. Mater.* **2005**, *17*, 621−625.

(10) Feng, S.; Huang, Y.; Wang, Q.; Qing, F.-L. Nonbiofouling Surface Based on Amphiphilic Alkanethiol Self-Assembled Monolayers. *Surf. Interface Anal.* **2011**, *43*, 770−776.

(11) Klein, E.; Kerth, P.; Lebeau, L. Enhanced Selective Immobilization of Biomolecules onto Solid Supports Coated with Semifluorinated Self-Assembled Monolayers. *Biomaterials* **2008**, *29*, 204−214.

(12) Bruce, R. C.; You, L.; Förster, A.; Pookpanratana, S.; Pomerenk, O.; Lee, H. J.; Marquez, M. D.; Ghanbaripour, R.; Zenasni, O.; Lee, T. R.; Hacker, C. A. Contrasting Transport and Electrostatic Properties of Selectively Fluorinated Alkanethiol Monolayers with Embedded Dipoles. *J. Phys. Chem. C* **2018**, *122*, 4881−4890.

(13) Ulman, A. Formation and Structure of Self-Assembled Monolayers. *Chem. Rev.* **1996**, *96*, 1533−1554.

(14) Love, J. C.; Estroff, L. A.; Kriebel, J. K.; Nuzzo, R. G.; Whitesides, G. M. Self-Assembled Monolayers of Thiolates on Metals as a Form of Nanotechnology. *Chem. Rev.* **2005**, *105*, 1103−1170.

(15) Vericat, C.; Vela, M. E.; Benitez, G.; Carro, P.; Salvarezza, R. C. Self-Assembled Monolayers of Thiols and Dithiols on Gold: New Challenges for a Well-Known System. *Chem. Soc. Rev.* **2010**, *39*, 1805−1834.

(16) Jamison, A. C.; Chinwangso, P.; Lee, T. R. Self−Assembled Monolayers: The Development of Functional Nanoscale Films. In *Functional Polymer Films*; Knoll, W., Advincula, R. C., Eds.; Wiley−VCH: Weinheim, 2011; Vol. *1*, pp 151−217.

(17) Barriet, D.; Lee, T. R. Fluorinated Self-Assembled Monolayers: Composition, Structure and Interfacial Properties. *Curr. Opin. Colloid Interface Sci.* **2003**, *8*, 236−242.

(18) Patole, S. N.; Baddeley, C. J.; O'Hagan, D.; Richardson, N. V.; Zerbetto, F.; Zotti, L. A.; Teobaldi, G.; Hofer, W. A. Self-Assembly of Semifluorinated *n*-Alkanethiols on (111)-Oriented Au Investigated with Scanning Tunneling Microscopy Experiment and Theory. *J. Chem. Phys.* **2007**, *127*, 024702.

(19) Alves, C. A.; Porter, M. D. Atomic Force Microscopic Characterization of a Fluorinated Alkanethiolate Monolayer at Gold and Correlations to Electrochemical and Infrared Reflection Spectroscopic Structural Descriptions. *Langmuir* **1993**, *9*, 3507−3512.

(20) Liu, G.-y.; Fenter, P.; Chidsey, C. E. D.; Ogletree, D. F.; Eisenberger, P.; Salmeron, M. An Unexpected Packing of Fluorinated *n*-Alkane Thiols on Au(111): A Combined Atomic Force Microscopy and X-Ray Diffraction Study. *J. Chem. Phys.* **1994**, *101*, 4301−4306.

(21) Chidsey, C. E. D.; Loiacono, D. N. Chemical Functionality in Self-Assembled Monolayers: Structural and Electrochemical Properties. *Langmuir* **1990**, *6*, 682−691.

(22) Colorado, R., Jr.; Graupe, M.; Shmakova, O. E.; Ramon, J. V.; Lee, T. R. Structural Properties of Self-Assembled Monolayers on Gold Generated from Terminally Fluorinated Alkanethiols. *ACS Symp. Ser.* **2001**, *781*, 276−292.

(23) Weinstein, R. D.; Moriarty, J.; Cushnie, E.; Colorado, R., Jr.; Lee, T. R.; Patel, M.; Alesi, W. R.; Jennings, G. K. Structure, Wettability, and Electrochemical Barrier Properties of Self-Assembled Monolayers Prepared from Partially Fluorinated Hexadecanethiols. *J. Phys. Chem. B* **2003**, *107*, 11626−11632.

(24) Yuan, Y.; Yam, C. M.; Shmakova, O. E.; Colorado, R., Jr.; Graupe, M.; Fukushima, H.; Moore, H. J.; Lee, T. R. Solution-Phase Desorption of Self-Assembled Monolayers on Gold Derived From Terminally Perfluorinated Alkanethiols. *J. Phys. Chem. C* **2011**, *115*, 19749−19760.

(25) Alloway, D. M.; Hofmann, M.; Smith, D. L.; Gruhn, N. E.; Graham, A. L.; Colorado, R., Jr.; Wysocki, V. H.; Lee, T. R.; Lee, P. A.; Armstrong, N. R. Interface Dipoles Arising from Self-Assembled Monolayers on Gold: UV−Photoemission Studies of Alkanethiols and Partially Fluorinated Alkanethiols. *J. Phys. Chem. B* **2003**, *107*, 11690−11699.

(26) Frey, S.; Heister, K.; Zharnikov, M.; Grunze, M.; Tamada, K.; Colorado, R., Jr.; Graupe, M.; Shmakova, O. E.; Lee, T. R. Structure of Self-Assembled Monolayers of Semifluorinated Alkanethiols on Gold and Silver Substrates. *Isr. J. Chem.* **2000**, *40*, 81−97.

(27) Fukushima, H.; Seki, S.; Nishikawa, T.; Takiguchi, H.; Tamada, K.; Abe, K.; Colorado, R., Jr.; Graupe, M.; Shmakova, O. E.; Lee, T. R. Microstructure, Wettability, and Thermal Stability of Semifluorinated Self-Assembled Monolayers (SAMs) on Gold. *J. Phys. Chem. B* **2000**, *104*, 7417−7423.

DOI: 10.1021/acs.chemmater.9b02887
Chem. Mater. 2020, 32, 953−968

(28) Graupe, M.; Takenaga, M.; Koini, T.; Colorado, R., Jr.; Lee, T. R. Oriented Surface Dipoles Strongly Influence Interfacial Wettabilities. *J. Am. Chem. Soc.* **1999**, *121*, 3222−3223.
(29) Colorado, R., Jr.; Lee, T. R. Physical Organic Probes of Interfacial Wettability Reveal the Importance of Surface Dipole Effects. *J. Phys. Org. Chem.* **2000**, *13*, 796−807.
(30) Tamada, K.; Ishida, T.; Knoll, W.; Fukushima, H.; Colorado, R., Jr.; Graupe, M.; Shmakova, O. E.; Lee, T. R. Molecular Packing of Semifluorinated Alkanethiol Self-Assembled Monolayers on Gold: Influence of Alkyl Spacer Length. *Langmuir* **2001**, *17*, 1913−1921.
(31) Bain, C. D.; Troughton, E. B.; Tao, Y. T.; Evall, J.; Whitesides, G. M.; Nuzzo, R. G. Formation of Monolayer Films by the Spontaneous Assembly of Organic Thiols from Solution onto Gold. *J. Am. Chem. Soc.* **1989**, *111*, 321−335.
(32) Zenasni, O.; Marquez, M. D.; Jamison, A. C.; Lee, H. J.; Czader, A.; Lee, T. R. Inverted Surface Dipoles in Fluorinated Self-Assembled Monolayers. *Chem. Mater.* **2015**, *27*, 7433−7446.
(33) Lee, H. J.; Jamison, A. C.; Lee, T. R. Surface Dipoles: A Growing Body of Evidence Supports Their Impact and Importance. *Acc. Chem. Res.* **2015**, *48*, 3007−3015.
(34) Leatherman, G.; Durantini, E. N.; Gust, D.; Moore, T. A.; Moore, A. L.; Stone, S.; Zhou, Z.; Rez, P.; Liu, Y. Z.; Lindsay, S. M. Carotene as a Molecular Wire: Conducting Atomic Force Microscopy. *J. Phys. Chem. B* **1999**, *103*, 4006−4010.
(35) Nozaki, K.; Munekane, M.; Yamamoto, T.; Ogawa, Y. X-ray and Thermal Studies on the Crystalline Phases of Normal Alkanethiols n-$C_nH_{2n+1}SH$ (n = 18, 19, 22, 23, 24). *J. Mater. Sci.* **2006**, *41*, 3935−3946.
(36) Porter, M. D.; Bright, T. B.; Allara, D. L.; Chidsey, C. E. D. Spontaneously Organized Molecular Assemblies. 4. Structural Characterization of *n*-Alkyl Thiol Monolayers on Gold by Optical Ellipsometry, Infrared Spectroscopy, and Electrochemistry. *J. Am. Chem. Soc.* **1987**, *109*, 3559−3568.
(37) Bain, C. D. Sum-Frequency Vibrational Spectroscopy of the Solid/Liquid Interface. *J. Chem. Soc., Faraday Trans.* **1995**, *91*, 1281−1296.
(38) Jacob, J. D. C.; Rittikulsittichai, S.; Lee, T. R.; Baldelli, S. Characterization of SAMs Derived from Octadecyloxyphenylethanethiols by Sum Frequency Generation. *J. Phys. Chem. C* **2013**, *117*, 9355−9365.
(39) Wang, H.-F.; Gan, W.; Lu, R.; Rao, Y.; Wu, B.-H. Quantitative Spectral and Orientational Analysis in Surface Sum Frequency Generation Vibrational Spectroscopy (SFG-VS). *Int. Rev. Phys. Chem.* **2005**, *24*, 191−256.
(40) Hirose, C.; Akamatsu, N.; Domen, K. Formulas for the Analysis of Surface Sum-Frequency Generation Spectrum by CH Stretching Modes of Methyl and Methylene Groups. *J. Chem. Phys.* **1992**, *96*, 997−1004.
(41) Hirose, C.; Yamamoto, H.; Akamatsu, N.; Domen, K. Orientation Analysis by Simulation of Vibrational Sum Frequency Generation Spectrum: CH Stretching Bands of the Methyl Group. *J. Phys. Chem.* **1993**, *97*, 10064−10069.
(42) Neese, F. The ORCA Program System. *Wiley Interdiscip. Rev.: Comput. Mol. Sci.* **2012**, *2*, 73−78.
(43) Kossmann, S.; Neese, F. Correlated ab Initio Spin Densities for Larger Molecules: Orbital-Optimized Spin-Component-Scaled MP2 Method. *J. Phys. Chem. A* **2010**, *114*, 11768−11781.
(44) Neese, F.; Schwabe, T.; Kossmann, S.; Schirmer, B.; Grimme, S. Assessment of Orbital-Optimized, Spin-Component Scaled Second-Order Many-Body Perturbation Theory for Thermochemistry and Kinetics. *J. Chem. Theory Comput.* **2009**, *5*, 3060−3073.
(45) Neese, F. An Improvement of the Resolution of the Identity Approximation for the Formation of the Coulomb Matrix. *J. Comput. Chem.* **2003**, *24*, 1740−1747.
(46) Weigend, F.; Ahlrichs, R. Balanced Basis Sets of Split Valence, Triple Zeta Valence and Quadruple Zeta Valence Quality for H To Rn: Design and Assessment of Accuracy. *Phys. Chem. Chem. Phys.* **2005**, *7*, 3297−3305.
(47) Biebuyck, H. A.; Bain, C. D.; Whitesides, G. M. Comparison of Organic Monolayers on Polycrystalline Gold Spontaneously Assembled from Solutions Containing Dialkyl Disulfides or Alkanethiols. *Langmuir* **1994**, *10*, 1825−1831.
(48) Nuzzo, R. G.; Dubois, L. H.; Allara, D. L. Fundamental Studies of Microscopic Wetting on Organic Surfaces. 1. Formation and Structural Characterization of a Self-Consistent Series of Polyfunctional Organic Monolayers. *J. Am. Chem. Soc.* **1990**, *112*, 558−569.
(49) Castner, D. G.; Hinds, K.; Grainger, D. W. X-ray Photoelectron Spectroscopy Sulfur 2p Study of Organic Thiol and Disulfide Binding Interactions with Gold Surfaces. *Langmuir* **1996**, *12*, 5083−5086.
(50) Ishida, T.; Hara, M.; Kojima, I.; Tsuneda, S.; Nishida, N.; Sasabe, H.; Knoll, W. High Resolution X-ray Photoelectron Spectroscopy Measurements of Octadecanethiol Self-Assembled Monolayers on Au(111). *Langmuir* **1998**, *14*, 2092−2096.
(51) *Surface Analysis: The Principal Techniques*, 2nd ed.; Vickerman, J. S., Gilmore, I. S., Eds.; John Wiley & Sons: Chichester, 2009.
(52) Lummerstorfer, T.; Hoffmann, H. IR Reflection Spectra of Monolayer Films Sandwiched between Two High Refractive Index Materials. *Langmuir* **2004**, *20*, 6542−6545.
(53) Barriet, D.; Chinwangso, P.; Lee, T. R. Can Cyclopropyl-Terminated Self-Assembled Monolayers on Gold Be Used to Mimic the Surface of Polyethylene? *ACS Appl. Mater. Interfaces* **2010**, *2*, 1254−1265.
(54) Snyder, R. G.; Strauss, H. L.; Elliger, C. A. Carbon-Hydrogen Stretching Modes and the Structure of *n*-Alkyl Chains. 1. Long, Disordered Chains. *J. Phys. Chem.* **1982**, *86*, 5145−5150.
(55) MacPhail, R. A.; Strauss, H. L.; Snyder, R. G.; Elliger, C. A. Carbon-Hydrogen Stretching Modes and the Structure of *n*-Alkyl Chains. 2. Long, All-Trans Chains. *J. Phys. Chem.* **1984**, *88*, 334−341.
(56) Durig, J. R.; Yu, Z.; Guirgis, G. A. Conformational Stability, Barriers to Internal Rotation, Vibrational Assignment, and ab initio Calculations of 2,2-Difluorobutane. *J. Mol. Struct.* **1999**, *509*, 115−135.
(57) Wenzl, I.; Yam, C. M.; Barriet, D.; Lee, T. R. Structure and Wettability of Methoxy-Terminated Self-Assembled Monolayers on Gold. *Langmuir* **2003**, *19*, 10217−10224.
(58) Greenler, R. G. Infrared Study of Adsorbed Molecules on Metal Surfaces by Reflection Techniques. *J. Chem. Phys.* **1966**, *44*, 310−315.
(59) Laibinis, P. E.; Bain, C. D.; Nuzzo, R. G.; Whitesides, G. M. Structure and Wetting Properties ω-Alkoxy-*n*-Alkanethiolate Monolayers on Gold and Silver. *J. Phys. Chem.* **1995**, *99*, 7663−7676.
(60) Asanuma, H.; Noguchi, H.; Huang, Y.; Uosaki, K.; Yu, H.-Z. Probing the Molecular Conformation of Self-Assembled Monolayers at Metal/Semiconductor Interfaces by Vibrational Sum Frequency Generation Spectroscopy. *J. Phys. Chem. C* **2009**, *113*, 21139−21146.
(61) Nishi, N.; Hobara, D.; Yamamoto, M.; Kakiuchi, T. Chain-Length-Dependent Change in The Structure of Self-Assembled Monolayers of *n*-Alkanethiols on Au(111) Probed by Broad-Bandwidth Sum Frequency Generation Spectroscopy. *J. Chem. Phys.* **2003**, *118*, 1904−1911.
(62) Laibinis, P. E.; Whitesides, G. M.; Allara, D. L.; Tao, Y. T.; Parikh, A. N.; Nuzzo, R. G. Comparison of the Structures and Wetting Properties of Self-Assembled Monolayers of *n*-Alkanethiols on the Coinage Metal Surfaces, Copper, Silver, and Gold. *J. Am. Chem. Soc.* **1991**, *113*, 7152−7167.
(63) Nelson, R. D.; Lide, D. R.; Maryott, A. A. Selected Values of Electric Dipole Moments for Molecules in the Gas Phase. *National Standard Reference Data Series National Bureau of Standards 10*, 1967.
(64) Smallwood, I. M. *Handbook of Organic Solvent Properties*; John Wiley & Sons: New York, 1996.

DOI: 10.1021/acs.chemmater.9b02887
Chem. Mater. 2020, 32, 953−968